Journal of Molecular Structure 1301 (2024) 137365

Contents lists available at ScienceDirect

Journal of Molecular Structure

journal homepage: www.elsevier.com/locate/molstr

New naphthoquinone thiazole hybrids as carbonic anhydrase and cholinesterase inhibitors: Synthesis, crystal structure, molecular docking, and acid dissociation constant

Cagla Efeoglu [a], Ozge Selcuk [a], Bunyamin Demir [b], Ertan Sahin [c], Hayati Sari [d], Cüneyt Türkeş [e], Yeliz Demir [f,*], Yahya Nural [a,*], Şükrü Beydemir [g,h]

[a] Department of Analytical Chemistry, Faculty of Pharmacy, Mersin University, TR-33169, Mersin, Türkiye
[b] Department of Mechanical Engineering, Faculty of Engineering, Mersin University, Mersin, 33169 Türkiye
[c] Department of Chemistry, Faculty of Science, Atatürk University, TR-25240 Erzurum, Türkiye
[d] Department of Chemistry, Faculty of Science and Arts, Gaziosmanpasa University, 60250 Tokat, Türkiye
[e] Department of Biochemistry, Faculty of Pharmacy, Erzincan Binali Yıldırım University, 24002 Erzincan, Türkiye
[f] Ardahan Univ, Nihat Delibalta Gole Vocational High School, Department of Pharmacy Services, 75700 Ardahan, Türkiye
[g] Department of Biochemistry, Faculty of Pharmacy, Anadolu University, 26470 Eskişehir, Turkey
[h] Bilecik Şeyh Edebali University, 11230 Bilecik, Türkiye

ARTICLE INFO

Keywords:
1,4-naphthoquinone
Thiazole
Enzyme inhibition
Crystal structure
Molecular docking
Acid dissociation constant

ABSTRACT

In this study, *N*-[3-(3-amino-1,4-dioxo-1,4-dihydronaphthalen-2-yl)-4-R-thiazol-2(3*H*)-ylidene]-2,6-difluorobenzamide derivatives as new 1,4-naphthoquinone thiazole hybrids were synthesized by reacting of *N*-[(3-amino-1,4-dioxo-1,4-dihydronaphthalen-2-yl)carbamothioyl]-2,6-difluorobenzamide with various α-bromoketones in 76–92% yields. Their molecular structures were characterized by ^{1}H NMR, ^{13}C NMR, ^{19}F NMR, FT-IR, and HRMS, and the stereochemistry of one of the hybrids was determined by single crystal x-ray diffraction study. These synthesized new compounds (**3a–e**) were found to be effective inhibitor molecules for cholinesterases (butyrylcholinesterase (BChE) and acetylcholinesterase (AChE)), and carbonic anhydrase I and II (*h*CA I and *h*CA II) enzymes. K_I values were found to be in the range of 45.03–84.43 nM for BChE, 26.12–98.42 nM for AChE, 67.86–161.60 nM for *h*CA I, and 55.27–87.48 nM for *h*CA II. The acid dissociation constants (pK_a) of 1,4-naphthoquinone thiazole hybrids were determined in 25% (v/v) DMSO:water (25.0 ± 0.1 °C, $I = 0.1$ M by NaCl). Three pK_a values for each hybrid were calculated with the HYPERQUAD program from the data obtained as a result of potentiometric titrations. The results obtained from molecular docking studies indicate that the compounds in question favorably fit within the active sites of *h*CAs and ChEs. Additionally, the acceptability of these compounds, as determined by Lipinski's and Jorgensen's rules, was estimated using the ADME/T results. Based on these estimations, it can be concluded that the synthesized molecules have the potential to be developed as effective and safe inhibitors of *h*CAs and ChEs, thus making them suitable lead agents for glaucoma and Alzheimer's disease.

1. Introduction

The hydration of CO_2 to protons and bicarbonate is catalyzed [1] by the well-known isoforms of carbonic anhydrases (CAs, EC 4.2.1.1) [2], which is essential for many pathologic and physiological processes in most organisms and tissues [3]. Organisms all over the phylogenetic tree express eight genetically distinct CA families, making their modulation a target for a diversity of diseases [4]. The clinical relevance of CA inhibitors (CAIs) extends to antitumor, antiepileptics, antiobesity diuretics, and antiglaucoma drugs [5]. They have recently become effective instruments for treating illnesses that aren't often treated with this group of pharmacological drugs, such as Alzheimer's disease (AD), oxidative stress, rheumatoid arthritis, cerebral ischemia, as anti-infective agents, and neuropathic pain [6].

A neurodegenerative brain disorder known as AD is affecting an increasing number of people, often characterized by cognitive debility

* Corresponding authors.
E-mail addresses: yelizdemir@ardahan.edu.tr (Y. Demir), yahyanural@mersin.edu.tr (Y. Nural).

https://doi.org/10.1016/j.molstruc.2023.137365
Received 6 November 2023; Received in revised form 13 December 2023; Accepted 18 December 2023
Available online 19 December 2023

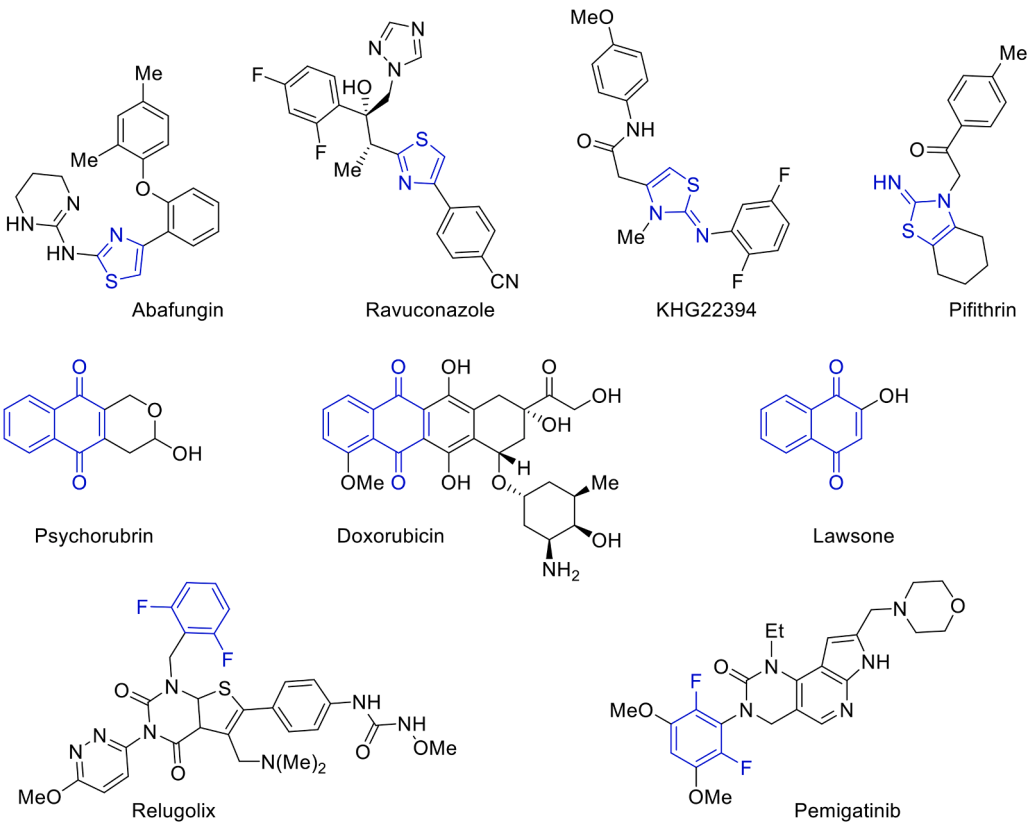

Fig. 1. Some pharmacologically active compounds containing thiazole, naphthoquinone or 2,6-difluorophenyl scaffold.

and memory loss [7]. The deterioration of brain functions, delusions, depression, neurodegeneration, anxiety, and apathy are among the primary symptoms of AD [8]. The significance of an accurate diagnosis becomes evident due to the absence of specific treatments for AD [9]. The disease is associated with two types of enzymes: acetylcholinesterase (AChE) and butyrylcholinesterase (BChE) [10]. Researchers have revealed that they can enhance the assembly of Aβ peptides into Alzheimer-type aggregates, thereby amplifying their neurotoxic effects [11]. Patients with AD exhibit abnormal levels of β-amyloid, aggregation of T proteins, inflammation, low levels of acetylcholine, and oxidative stress [12]. Current research on AD predominantly interest in the cholinergic system, with a primary focus on AChE inhibitors [13].

The thiazole pharmacophore has a critical place in drug research and development studies, as many compounds containing thiazole core, such as abafungin, ravuconazole, [14,15], pifithrin, and KHG22394 [16] (Fig. 1), are available on the market as drugs or are in clinical trials. It is known that thiazole derivatives show a wide range of pharmacological activities such as anticancer [17], antioxidant [18], DNA Cleavage [19], antibacterial [20,21], antimycobacterial [22,23], and antifungal [24,25] activities as well as kinase [26] α-glucosidase [27,28], and α-amylase [28,29] enzyme inhibitory activity. Additionally, there are many studies showing that thiazoles act as CAs [30,31], AChE [30,32,33], and BChE [32,33] enzyme inhibitors.

The naphthoquinone moiety is one of the most popular pharmacophore groups in medicinal chemistry, as many biologically important naphthoquinone derivatives such as doxorubicin, psychorubrin, and lawsone (Fig. 1) [34] are known. Naphthoquinones exhibit a wide range of biological activity such as anti-inflammatory [35,36], DNA cleavage [37], anticancer [38] antiviral [39], antimicrobial [40], antimycobacterial [41], and antimalarial [42] activities. Moreover, compounds bearing 1,4-naphthoquinone scaffold are known to exhibit enzyme inhibitory activity of CAs [43], AChE [43,44], and BChE [43,44]
.

As of today, many drugs available on the markets such as avapritinib, selumetinib, rimegepant, and berotralstat contain at least one fluorine atom in their core structure. Moreover, today, there are also many drugs on the market that contain 2,6-fluorophenyl moiety in their structures, such as relugolix and pemigatinib (Fig. 1) [45]. Compounds containing 2,6-flourophenyl core are known to exhibit a wide range pharmacological activities such as anti-inflammatory [36], anticancer [46], and antibacterial [47] as well as various enzyme inhibitory activities such as store-operated calcium channel [48] and kinase [49] inhibitors. In addition, in our previous studies, glutathione S-transferases (GST) and glutathione reductase (GR) enzyme inhibition activities of various thioureas containing *o, m, p*-flourophenyl, 2,5-difluorophenyl and 2,6-difluorophenyl were examined. We reported that the 1-(2,6-difluorophenyl)thiourea showed more of inhibitory activities against GST and GR enzymes than others [50].

Herein, we report the synthesis of new naphthoquinone thiazole hybrids bearing 2,6-difluorophenyl and the investigation on the enzyme inhibitory activities towards hCAs, AChE, and BChE. The effects of the synthesized inhibitors on the activity of these enzymes were examined to discover their potential to be used as drug precursors for conditions such as glaucoma or Alzheimer's disease. Structure of *N*-[3-(3-amino-1,4-dioxo-1,4-dihydronaphthalen-2-yl)−4-phenylthiazol-2(3*H*)-ylidene]-2,6-difluorobenzamide was proved by single crystal x-ray diffraction analysis. Molecular docking calculations of molecules and their affinities towards the crystal structures of the studied enzymes were employed. Also, determination of pK_a values, which is of critical importance in pharmaceutical R&D studies, is also reported.

2. Experimental

2.1. Materials and instrumentation

The precursor chemicals used were purchased from Merck or Aldrich

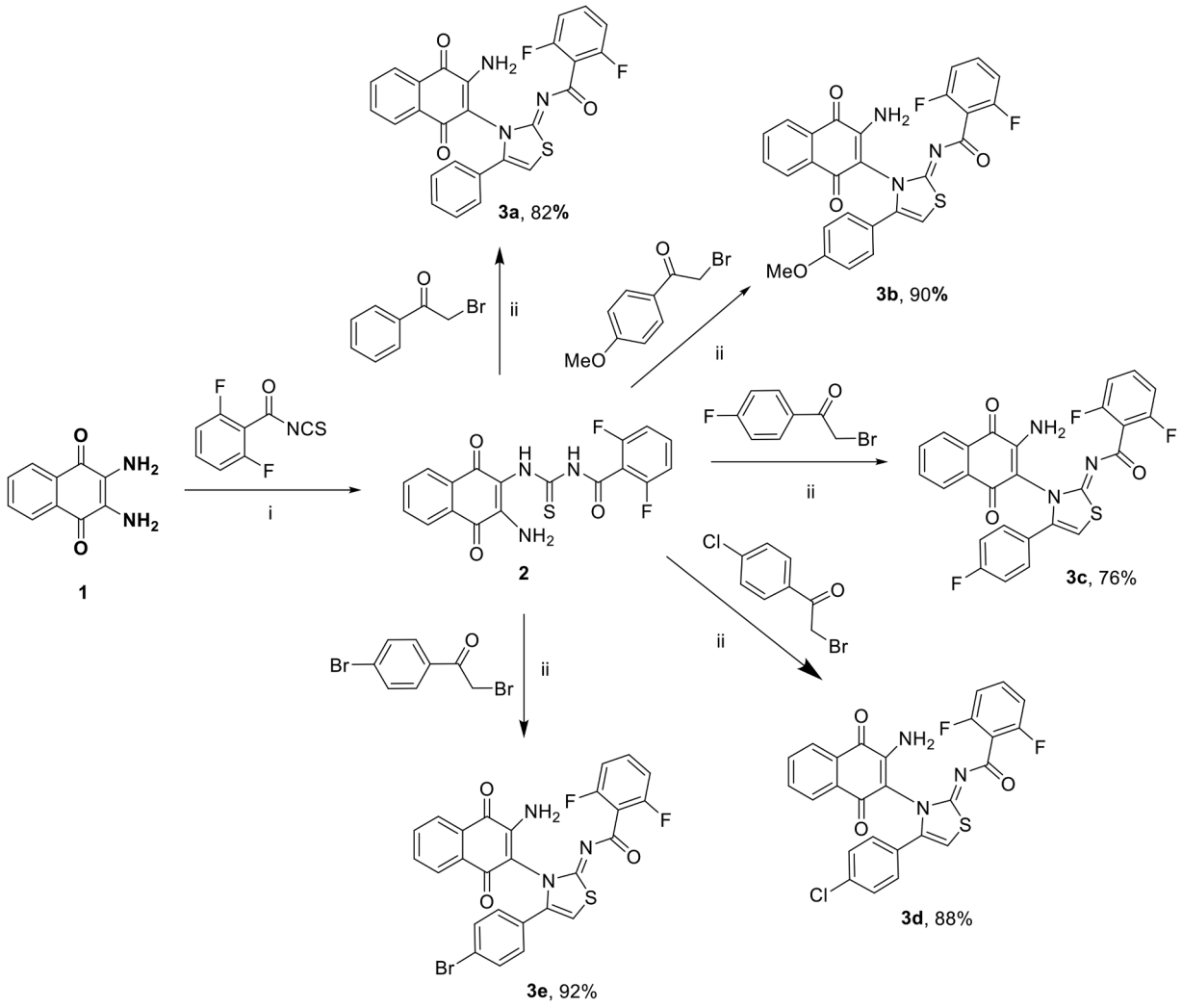

Scheme 1. Synthesis of 1,4-naphthoquinone thiazole hybrids (**3a–e**). **i.** Acetone, reflux, 18 h; **ii.** Acetone, reflux, 48 h.

and were used without any purification because they were of high quality. A Mattson 1000 Fourier transform infrared (FT-IR) spectrophotometer and a nuclear magnetic resonance (NMR) spectrophotometer from Bruker Ultrashield Plus Biospin GmbHt at 400 MHz were used to record the FT-IR and NMR spectra, respectively. The NMR spectra of the compounds were determined in dimethyl sulfoxide-d6 and chemical shifts were given in parts per million (δ) in the field from TMS as using internal standard. The following abbreviations are used; *s* = Singlet, *d* = Doublet, dd = Doublet of doublets, *m* = Multiplet. High resolution mass (HRMS) spectra were recorded using an Agilent Technologies 6224 TOF LC/MS instrument. Melting points were determined by a Mettler Toledo MP90. pH-metric titrations were performed using a Titroline 7000 automatic titrator with SI-Analytics combined with a glass pH electrode that can be controlled by a computer and contains an automatic microburette.

2.2. Synthesis of the N-[(3-amino-1,4-dioxo-1,4-dihydronaphthalen-2-yl)carbamothioyl]-2,6-difluorobenzamide **2**

The *N*-[(3-amino-1,4-dioxo-1,4-dihydronaphthalen-2-yl)carbamothioyl]-2,6-difluoro benzamide was synthesized by the reaction of 2,3-diaminonaphthalene-1,4-dione **1** with 2,6-difluorobenzoyl isothiocyanate in acetone at reflux temperature as described previously [51]. Yellow powder. Yield, 0.35 g, 90%. m.p.: 228–231 °C (decomp.). ^{1}H NMR (400 MHz, DMSO-d_6): δ 12.23 (s, 1H, NH), 11.24 (s, 1H, NH), 8.03 – 7.99 (m, 2H, Ar–H), 7.88 – 7.85 (m, 1H, Ar–H), 7.78 – 7.75 (m, 1H, Ar–H), 7.68 – 7.60 (m, 1H, Ar–H), 7.47 (s, 2H, NH_2), 7.28 – 7.24 (m, 2H, Ar–H). ^{13}C NMR (100 MHz, DMSO-d_6): δ 181.6, 179.8, 176.7, 161.1, 159.0 (dd, J_{FC} = 250.6, 7.0 Hz, 2 x C), 144.8, 135.1, 133.3 (dd, J_{FC} = 10.2, 9.7 Hz, C), 132.5, 132.4, 130.1, 125.9, 125.7, 113.3 (dd, J_{FC} = 21.1, 20.9 Hz C), 112.8, 112.0 (d, J_{FC} = 19.5, 4.5 Hz, 2 x C).

2.3. General procedure for the synthesis of 1,4-naphthoquinone thiazole hybrids bearing 2,6-difluorophenyl **3a–e**

A solution of corresponding 2-bromo-1-substituted ethanone (1.2 mmol) in acetone (30 mL) was added dropwise to the stirred solution of *N*-[(3-amino-1,4-dioxo-1,4-dihydronaphthalen-2-yl)carbamothioyl]-2,6-difluoro benzamide **2** (0.39 g, 1 mmol) in acetone (50 mL) at room temperature, and heated to reflux temperature (Scheme 1). After determining by TLC that the reaction was complete after 48 h, the reaction solvent was evaporated under reduced pressure. The crude mixture was washed several times with saturated sodium bicarbonate and then with diethyl ether and methanol until the final products were obtained in pure form. Molecular structures of the desired products **3a–e** were characterized by ^{1}H NMR, ^{13}C NMR, ^{19}F NMR, FT-IR, and HRMS (Figs. S1–S25).

2.3.1. N-[3-(3-amino-1,4-dioxo-1,4-dihydronaphthalen-2-yl)-4-phenylthiazol-2(3H)-ylidene]-2,6-difluorobenzamide, **3a**

Orange powder. Yield, 0.40 g, 82%. m.p.: 273–275 °C (decomp.). IR (cm^{-1}): υ_{max} 3389, 3298, 3266, 3168, 3121, 3056, 1690, 1646, 1611, 1588, 1568, 1557, 1463, 1441. ^{1}H NMR (400 MHz, DMSO-d_6): δ 8.29 (s, 1H, NH), 7.96 (d, 1H, J = 7.4 Hz, Ar–H), 7.85–7.70 (m, 4H, Ar–H and N—H), 7.40–7.32 (m, 1H, Ar–H), 7.32 (s, 5H, Ar–H), 7.23 (s, 1H, thiazole C—H), 7.05–7.01 (m, 2H, Ar–H). ^{13}C NMR (100 MHz, DMSO-d_6): δ 180.8 (C═O), 175.7 (C═O), 169.6 (C═O), 168.4, 159.2 (dd, J_{FC} = 250.0 Hz, 7.9 Hz, 2 x C-F), 147.0, 139.6, 135.6, 132.9, 131.7, 130.9, (dd, J_{FC} = 11.5 Hz, 9.3 Hz, C), 130.1, 129.8, 129.3, 128.3 (2 x C), 128.1 (2 x C), 126.4, 125.9, 117.9 (dd, J_{FC} = 20.5 Hz, 20.5 Hz, C), 111.9 (dd, J_{FC} = 19.1 Hz, 5.6 Hz, 2 x C), 111.6, 107.9. ^{19}F NMR (376 MHz, DMSO-d_6): δ −112.9 (t, 2F, 2 x CF). HRMS (ESI-TOF-MS): calcd. for $C_{26}H_{16}F_2N_3O_3S$ [M+H$^+$] 488.0875; found 488.0874.

2.3.2. N-[3-(3-amino-1,4-dioxo-1,4-dihydronaphthalen-2-yl)-4-(4-methoxyphenyl)thiazol-2(3H)-ylidene]-2,6-difluorobenzamide **3b**

Yellow powder. Yield, 0.47 g, 90%. m.p.: 285–287 °C (decomp.). IR (cm^{-1}): υ_{max} 3391, 3300, 3267, 3175, 3122, 3066, 1694, 1648, 1615, 1589, 1572, 1506, 1461, 1441. ^{1}H NMR (400 MHz, DMSO-d_6): δ 8.24 (s, 1H, NH), 7.97 (d, 1H, J = 6.8 Hz, Ar–H), 7.87–7.71 (m, 4H, Ar–H and N—H), 7.42–7.34 (m, 1H, Ar–H), 7.24 (d, 2H, J = 8.8 Hz, Ar–H), 7.13 (s, 1H, thiazole C—H), 7.04–7.00 (m, 2H, Ar–H), 6.88 (d, 2H, J = 8.8 Hz, Ar–H). ^{13}C NMR (100 MHz, DMSO-d_6): δ 180.8 (C═O), 175.7 (C═O), 169.4 (C═O), 168.2, 159.9, 159.2 (dd, J_{FC} = 248.3 Hz, 7.6 Hz, 2 x C-F), 147.0, 139.5, 135.6, 132.9, 131.7, 130.9, (dd, J_{FC} = 11.2 Hz, 9.0 Hz, C), 129.8, 129.6 (2 x C), 126.4, 125.9, 122.2, 117.9 (dd, J_{FC} = 20.4 Hz, 20.4 Hz, C), 113.7 (2 x C), 111.9 (dd, J_{FC} = 19.2 Hz, 5.7 Hz, 2 x C), 111.7, 107.3, 55.1. ^{19}F NMR (376 MHz, DMSO-d_6): δ −112.9 (t, 2F, 2 x CF). HRMS (ESI-TOF-MS): calcd. for $C_{27}H_{18}F_2N_3O_4S$ [M+H$^+$] 518.0981; found 518.0998.

2.3.3. N-[3-(3-amino-1,4-dioxo-1,4-dihydronaphthalen-2-yl)-4-(4-fluorophenyl)thiazol-2(3H)-ylidene]-2,6-difluorobenzamide **3c**

Green powder. Yield, 0.38 g, 76%. m.p.: 269–271 °C (decomp.). IR (cm^{-1}): υ_{max} 3400, 3307, 3275, 3225, 3119, 3063, 1698, 1649, 1609, 1593, 1571, 1557, 1504, 1462, 1442. ^{1}H NMR (400 MHz, DMSO-d_6): δ 8.30 (s, 1H, NH), 7.97 (dd, 1H, J = 7.6 Hz, 0.8 Hz, Ar–H), 7.86–7.71 (m, 4H, Ar–H and N—H), 7.43–7.33 (m, 3H, Ar–H), 7.24 (s, 1H, thiazole C—H), 7.22–7.17 (m, 2H, Ar–H), 7.05–7.01 (m, 2H, Ar–H). ^{13}C NMR (100 MHz, DMSO-d_6): δ 180.7 (C═O), 175.7 (C═O), 169.5 (C═O), 168.4, 162.5 (d, J_{FC} = 246.8 Hz, C-F), 159.2 (dd, J_{FC} = 249.2 Hz, 7.7 Hz, 2 x C-F), 147.0, 138.5, 135.6, 132.9, 131.6, 130.9 (dd, J_{FC} = 11.4 Hz, 10.1 Hz, C), 130.5, 130.4, 129.8, 126.5 (d, J_{FC} = 3.2 Hz, C), 126.4, 125.9, 117.8 (dd, J_{FC} = 20.5 Hz, 20.4 Hz, C), 115.5, 115.3, 111.9 (dd, J_{FC} = 19.1 Hz, 5.8 Hz, 2 x C), 111.3, 108.2. ^{19}F NMR (376 MHz, DMSO-d_6): δ −111.6 (m, 1F, CF), −112.9 (t, 2F, 2 x CF). HRMS (ESI-TOF-MS): calcd. for $C_{26}H_{15}F_3N_3O_3S$ [M+H$^+$] 506.0781; found 506.0807.

2.3.4. N-[3-(3-amino-1,4-dioxo-1,4-dihydronaphthalen-2-yl)-4-(4-chlorophenyl)thiazol-2(3H)-ylidene]-2,6-difluorobenzamide **3d**

Black powder. Yield, 0.46 g, 88%. m.p.: 246–248 °C (decomp.). IR (cm^{-1}): υ_{max} 3425, 3295, 3254, 3155, 3063, 1687, 1644, 1620, 1587, 1572, 1557, 1463, 1445. ^{1}H NMR (400 MHz, DMSO-d_6): δ 8.31 (s, 1H, NH), 7.98 (d, 1H, J = 7.4 Hz, Ar–H), 7.86–7.72 (m, 4H, Ar–H and N—H), 7.44–7.29 (m, 6H, Ar–H, thiazole C—H), 7.09–6.96 (m, 2H, Ar–H). ^{13}C NMR (100 MHz, DMSO-d_6): δ 180.7 (C═O), 175.7 (C═O), 169.5 (C═O), 168.4, 159.9, 159.2 (dd, J_{FC} = 250.2 Hz, 7.6 Hz, 2 x C-F), 147.1, 138.3, 135.6, 134.1, 132.9, 131.0 (dd, J_{FC} = 10.7 Hz, 9.5 Hz, C), 129.9 (2 x C), 129.8, 129.0, 128.5 (2 x C), 126.4, 125.9, 117.8 (dd, J_{FC} = 20.3 Hz, 20.3 Hz, C), 111.9 (dd, J_{FC} = 18.8 Hz, 5.5 Hz, 2 x C), 111.3, 108.6. ^{19}F NMR (376 MHz, DMSO-d_6): δ −112.8 (s, 2F, 2 x CF). HRMS (ESI-TOF-MS): calcd. for $C_{26}H_{15}ClF_2N_3O_3S$ [M+H$^+$] 522.0485; found 522.0508.

2.3.5. N-[3-(3-amino-1,4-dioxo-1,4-dihydronaphthalen-2-yl)-4-(4-bromophenyl)thiazol-2(3H)-ylidene]-2,6-difluorobenzamide **3e**

Yellow powder. Yield, 0.52 g, 92%. m.p.: 275–277 °C (decomp.). IR (cm^{-1}): υ_{max} 3420, 3295, 3246, 3155, 3058, 1686, 1643, 1619, 1594, 1585, 1571, 1557, 1476, 1462. ^{1}H NMR (400 MHz, DMSO-d_6): δ 8.33 (s, 1H, NH), 7.96 (d, 1H, J = 7.4 Hz, Ar–H), 7.85–7.69 (m, 4H, Ar–H and N—H), 7.57–7.55 (m, 2H, Ar–H), 7.41–7.34 (m, 1H, Ar–H), 7.31–7.26 (m, 3H, thiazole C—H, Ar–H), 7.04–7.01 (m, 2H, Ar–H). ^{13}C NMR (100 MHz, DMSO-d_6): δ 180.8 (C═O), 175.8 (C═O), 169.6 (C═O), 168.5, 159.3 (dd, J_{FC} = 250.1 Hz, 7.6 Hz, 2 x C-F), 147.2, 138.4, 135.6, 132.9, 131.7, 131.5 (2 x C), 131.0 (dd, J_{FC} = 10.5 Hz, 10.0 Hz, C), 130.2 (2 x C), 129.9, 129.4, 126.4, 125.9, 117.8 (dd, J_{FC} = 20.2 Hz, 20.2 Hz, C), 112.0 (dd, J_{FC} = 18.9 Hz, 5.4 Hz, 2 x C), 111.3, 108.6. ^{19}F NMR (376 MHz, DMSO-d_6): δ −112.9 (t, 2F, 2 x CF). HRMS (ESI-TOF-MS): calcd. for $C_{26}H_{15}BrF_2N_3O_3S$ [M+H$^+$] 565.9980; found 565.9969.

2.4. X-ray diffraction analysis

For the crystal structure determination, single-crystal of the compound **3a** was used for data collection on a Bruker APEX-II D8 Venture CCD diffractometer. Graphite-monochromated Mo-Kα radiation (λ = 0.71,073 Å) and ω- and φ-scans technique with Δw = 5° for one image were used for data collection. The lattice parameters were determined by the least-squares methods on the basis of all reflections with $F^2 > 2\sigma(F^2)$. Data collection was carried out by APEX2 [52], cell refinement and data reduction were carried out by Bruker SAINT Software [52]. The structures were solved by direct methods using SHELXS-2013 [53], which allowed for the location of most of the heaviest atoms, with the remaining non-hydrogen atoms being located from different Fourier maps calculated from successive full-matrix least squares refinement cycles on F^2 using SHELXL-2013 [53]. All non-hydrogen atoms were refined using anisotropic displacement parameters. Hydrogens attached to carbons were located at their geometric positions using appropriate HFIX instructions in SHELXL. The final difference Fourier maps showed no peaks of chemical significance. Crystal data for **3a**: $C_{26}H_{15}F_2N_3O_3S$, crystal system, space group: triclinic, *P*-1; (no:2); unit cell dimensions: a = 7.8213(5), b = 12.7259(8), c = 13.*0253*(8) Å, α= 63.243(2), β= 82.055(2), γ= 72.967(3)°; volume; 1106.82(4) Å^3, formula weight; 487.47, Z = 2; calculated density: 1.463 g/cm^3; absorption coefficient: 1.761 mm^{-1}; F (000): 500; θ-range for data collection 3.0–72.4°; refinement method: full matrix least-square on F^2; data/parameters: 4371/317; goodness-of-fit on F^2: 1.029; final R-indices [$I > 2\ \sigma(I)$]: R_1= 0.082, wR_2= 0.214; largest diff. peak and hole: 1.102 and −0.583 e Å^{-3}.

CCDC-2304128 number contains the supplementary crystallographic data for compound **3a**. These data are provided free of charge via the joint CCDC/FIZ Karlsruhe deposition service, www.ccdc.cam.ac.uk/structures

2.5. Enzyme inhibition study

The inhibition effects of compounds versus the esterase activity of the *h*CAs were determined by following the change in absorbance at 348 nm according to the assay defined by Verpoorte et al. [54] *h*CAs's activities were measured using 4-nitrophenyl acetate as previous study [55,56]. All the measurements were repeated thrice. AChE activity was assessed using a modified version of Ellman's method [57]. The measurement of ChEs activity was conducted with acetylthiocholine/butyrylthiocholine iodide as substrates, along with 5, 5-dithiobis(2-nitrobenzoic)acid. Substrate utilization was monitored spectrophotometrically at 412 nm [58]. The inhibitory effects of the newly synthesized compounds were assessed using a minimum of five different inhibitor concentrations for *h*CAs and ChEs. The IC_{50} values for these synthesized derivatives were determined from the graphs of Activity (%) versus for each compound (**3a–e**) [59]. Inhibition types and K_I values were determined using Lineweaver and Burk's curves [60].

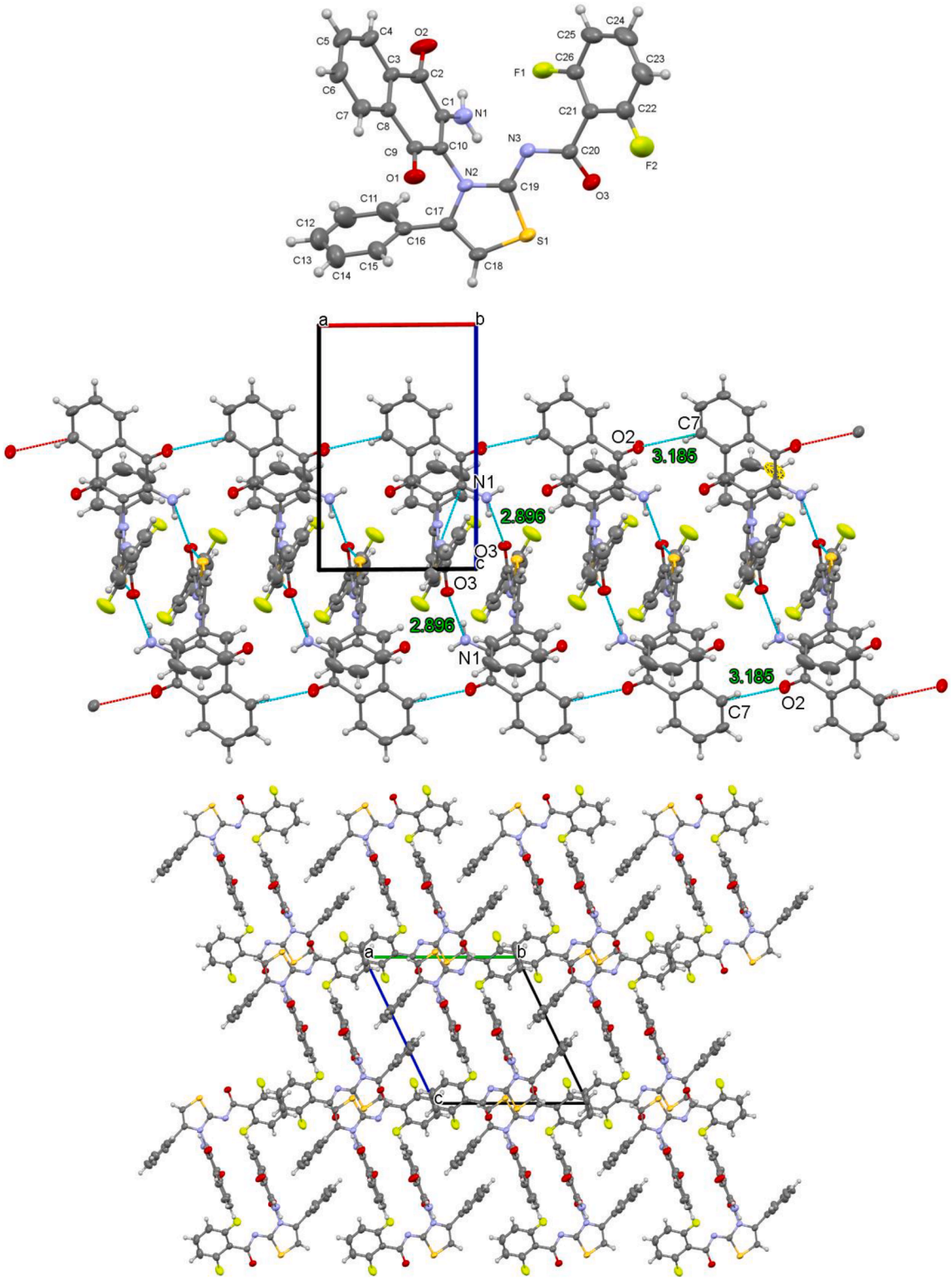

Fig. 2. (Up) The molecular structure of **3a** with displacement ellipsoids at the 40% probability level. (Mid.) Infinite dimeric chain structure of **3a** propagating along the b-axis direction via hydrogen bonds (dotted turquoise and red lines). (Down) The crystal packing viewed down along the *a*-axis.

2.6. Statistical study

Analysis of enzyme inhibition data and generation of graphs were performed using GraphPad Prism version 9 (GraphPad Software, La Jolla, California, USA) for Mac. The K_I values were calculated using SigmaPlot, version 12 (Systat Software, San Jose, California, USA) for Windows. Statistical comparisons between data sets were performed using the extra sum-of-squares *F* test and the AIC approach. Statistical significance was determined when the *p*-value was less than 0.05. The results were presented as mean ± standard error of the mean (95% confidence intervals).

Table 1
K_I values of 1,4-naphthoquinone thiazole hybrids on studied enzymes.

Comp. ID	*h*CA I		*h*CA II		AChE		BChE	
	K_I (nM)	R^2	K_I (nM)	R^2	K_I (nM)	R^2	K_I (nM)	R^2
3a	142.30 ± 16.32	0.9839	79.49 ± 9.54	0.9803	27.46 ± 2.86	0.9801	63.67 ± 5.74	0.9852
3b	109.90 ± 13.03	0.9827	55.27 ± 5.92	0.9841	85.57 ± 7.50	0.9858	55.19 ± 5.44	0.9804
3c	161.60 ± 20.19	0.9857	62.36 ± 8.09	0.9808	73.57 ± 6.11	0.9876	45.03 ± 3.72	0.9863
3d	67.86 ± 8.06	0.9815	56.85 ± 6.79	0.9837	98.42 ± 8.70	0.9861	69.27 ± 5.91	0.9850
3e	85.14 ± 9.39	0.9839	87.48 ± 11.76	0.9808	26.12 ± 2.54	0.9831	84.43 ± 7.73	0.9869
AAZ [a]	20.52± 3.17	0.9812	23.77± 4.01	0.9891				
THA [b]					81.21± 10.45	0.9788	73.13± 13.67	0.9788

[a] Acetazolamide.
[b] Tacrine.

2.7. Computational study

The latest edition of the Small-Molecule Drug Discovery Suite for Mac, version 2023-3, was utilized to perform molecular docking analysis in this study. The protein data bank (PDB) IDs, 1AZM [61,62], 3HS4 [63,64], 7XN1 [65,66], and 4BDS [67,68] were obtained from the RCSB Protein Data Bank and were used as models for the experiment, representing *h*CA I and II isoforms, AChE, and BChE, respectively. These structures were prepared for docking using the Protein Preparation Wizard [69,70] of this suite. The molecule structures of new 1,4-naphthoquinone thiazole hybrids (**3a–e**) were sketched using the ChemDraw program, version 21 (PerkinElmer, Inc., Waltham, MA, USA) for Mac, and then optimized using the LigPrep module [71,72] at pH 7.4 ± 0.5 in the OPLS4 force field [73,74] with Epik [75,76]. The active site residues verified by the SiteMap tool [77–79] were defined in the Receptor Grid Generation [80,81] module to generate the receptor grid in the Maestro panel [82,83]. The Glide application [84,85] was utilized with default settings in the extra precision (XP) method [86,87] to dock the most effective inhibitors to *h*CAs and ChEs. Furthermore, the QikProp tool [88,89] was employed to forecast the ADME/T (absorption, distribution, metabolism, elimination, and toxicity) characteristics of all targeted molecules (**3a–e**) in this investigation.

2.8. Determination of acid dissociation constants

Determination of the pK_a values of **3a–e** was potentiometrically performed at 25.0 ± 0.1 °C in 25% (*v/v*) DMSO:water at an ionic strength of 0.1 M NaCl using a previously described method [90]. Stock solutions of **3a–e** were prepared as 1×10^{-3} M in DMSO, and stock solutions of 0.025 M NaOH, 0.1 M HCl and 1 M NaCl were prepared using deionized water. While potentiometric titrations were performed with the help of a computer-controlled automatic titrator, the temperature of the double-walled glass titration cell was kept constant at 25.0 ± 0.1 °C using a thermostat. Throughout the titration, the solution was stirred at a constant speed using a magnetic stirrer and nitrogen gas was passed through. After adding 10 mL of the stock solution of **3a–e** ligands to the titration cell, 2.5 mL of DMSO was added. Then, 1 mL 0.1 M HCl, 5 mL 1 M NaCl stock solutions and 31.5 mL deionized water were added to the titration cell containing the ligand, respectively. While the solution was mixed at constant speed, the lid of the titration cell was sealed, and the titration process was started after nitrogen gas was passed through for at least 3 min. The pK_w value was obtained as 14.52± 0.05 at the ionic strength employed.

3. Results and discussion

3.1. Synthesis and characterization

The new naphthoquinone thiazole hybrids bearing 2,6-difluorophenyl **3a–e** were obtained by the reaction of *N*-[(3-amino-1,4-dioxo-1,4-dihydronaphthalen-2-yl)carbamothioyl]-2,6-difluorobenzamide **2** and corresponding α-bromoketones in acetone at refluxing temperature in 76–92% yields (Scheme 1). The intermediate *N*-[(3-amino-1,4-dioxo-1,4-dihydronaphthalen-2-yl)carbamothioyl]-2,6-difluorobenzamide **2** were prepared by reacting 2,3-diaminonaphthalene-1,4-dione **1** with 2,6-difluorobenzoyl isothiocyanate as described previously [51]. Molecular structures of the products **3a–e** were characterized by ^{1}H NMR, ^{13}C NMR, ^{19}F NMR, FT-IR, and HRMS (Figs. S1–S20), and stereochemistry of **3a** was determined by single crystal x-ray diffraction (Fig. 2). ^{1}H NMR spectra of **3a–e**, the characteristic singlet peak of the thiazole core proton was observed in the range of 6.82 – 7.44 ppm. The NH peaks of C(O)NHC(S)NH moiety, observed as singlets at 12.23 ppm and 11.24 ppm in the ^{1}H NMR spectrum of intermediate **2,** disappeared as expected in the ^{1}H NMR spectra of **3a–e** due to thiazole formation. NH_2 protons were observed as a single peak at 7.47 ppm in the ^{1}H NMR spectrum of **2** [51]. Due to one of the protons of NH_2 forming a hydrogen bond with the benzamide moiety, NH_2 protons were observed as single peaks in different regions in the ^{1}H NMR spectra of **3a–e**. In addition, the C═O carbon of 2,6-difluorobenzamide group, which was observed at 161.1 ppm in the ^{13}C NMR spectrum of **2**, was observed in the range of 170.8 – 169.4 ppm for the compounds **3a–e**. In the ^{19}F NMR spectra of **3a–e**, the peaks belonging to the F atoms located in the 2 and 6 positions of the phenyl ring were observed at approximately −112.9 ppm. In the ^{19}F NMR spectrum of **3c**, which also contains a phenyl ring with a fluorine atom in the para position, the peak of the fluorine atom was observed at −111.6 ppm. Most notably, unlike **2a**, C═N stretching vibration peaks were observed in the FT-IR spectrum of **3a–e** in the range of 1649 – 1643 cm^{-1} due to the formation of 2-iminothiazole scaffold.

Crystal structure: The molecular structure of *N*-[3-(3-amino-1,4-dioxo-1,4-dihydronaphthalen-2-yl)-4-phenylthiazol-2(3*H*)-ylidene]-2,6-difluorobenzamide **3a** was characterized by single crystal x-ray diffraction analysis (Fig. 2). Compound **3a** crystallized as orange prisms in acetone solvent and was solved in the monoclinic space group *P*-1 with two molecules in the unit cell. The structure of **2** was previously solved by x-ray diffraction analysis [51]. Here, starting from molecule **2**, the cyclization product resulting from the reaction with α-bromoketone is clearly seen. Compound **3a** has fluorobenzene, aminonaphthoquinone, and phenyl groups at consecutive positions of thiazole heterocycle. Thiazole ring is planar. Phenyl and naphthoquinone rings are significantly rotated relative to thiazole ring with dihedral angles of 66.1° (C3/C8), 69.3° (C11/C16) and 31.8° (C21/C26). Deviation from planarity of the molecule is due to significant steric effects and intermolecular interactions. In the thiazole moiety, bond lengths S1-C19 1.722(3) Å and S1-C18 1.716(3) Å indicate single bond character, N2-C17 1.390(3) Å and N2-C19 1.372(3) Å bonds are single bonds. C17-C18 1.351(3) length is double. All this indicates that the higher aromaticity of thiazole is due to delocalization of a lone pair of sulfur electrons across the ring.

In the crystal, the molecules form *H*-bonded centrosymmetric dimers. The effective hydrogen bond occurs between the O atoms of the fluorobenzene carbonyl and the amino group, N1-*H*···O3 [*D*···*A* = 2.896 (3) Å] with an *R*(18) synthon. These dimeric units form a polymeric structure with adjacent dimers. The hydrogen bond C7-*H*···O2, *d*(*D*···*A*) distances of 3.185(3) Å causes the formation of this polymeric dimers

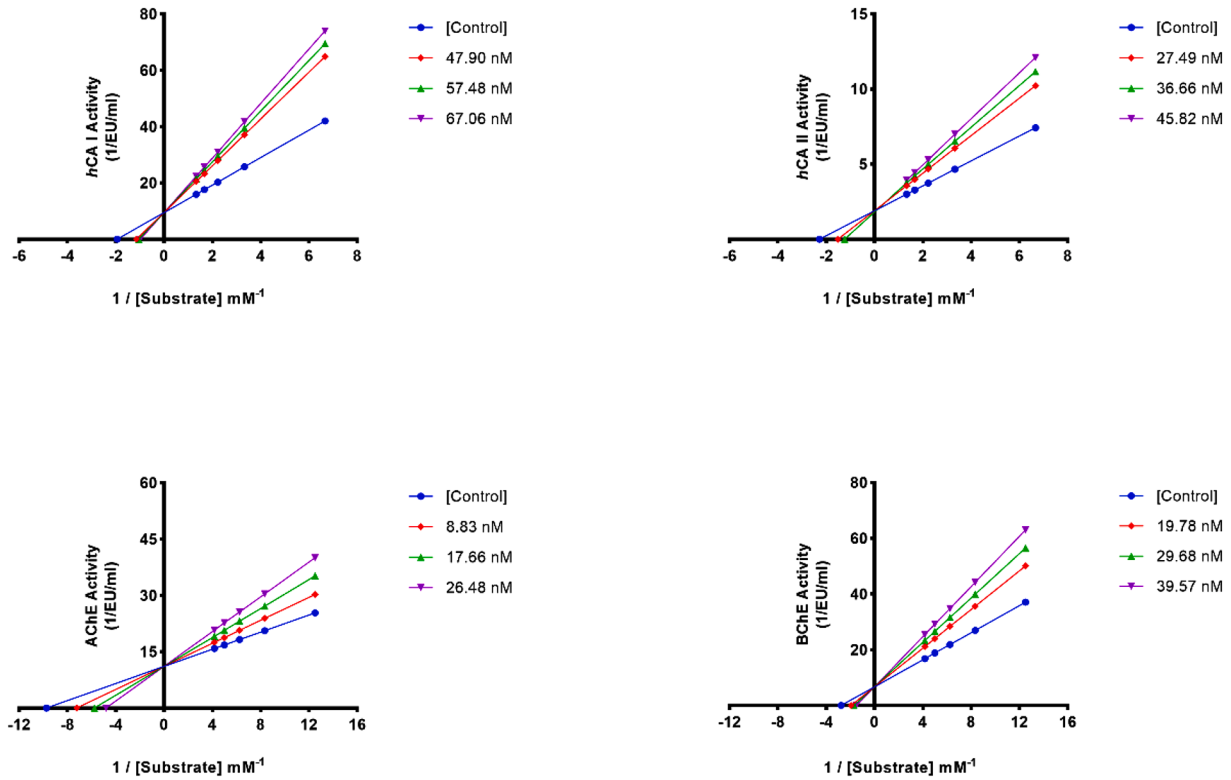

Fig. 3. Lineweaver-Burk graphs of the most potent inhibitors, **3d** (for *h*CAs), **3e**, and **3c** (for AChE and BChE).

(Fig. 2). The π-π stacking interactions between the delocalized π-electrons of the phenyl rings are weak. The distance between the rings centroids are in the range of 3.55–5.75 Å. Along with that, vdW interactions contribute to the formation of stable structures.

3.2. Enzyme inhibition study

The influences of 1,4-naphthoquinone thiazole hybrid derivatives against *h*CAs, AChE and BChE were analysed using an *in vitro* inhibition investigation. The obtained results (K_I values) for all the synthesized compounds (**3a–e**) and standard inhibitors (acetazolamide; AAZ and tacrine; THA) are tabulated in Table 1.

i) CAIs display a variety of bioactivities linked to numerous diseases, including osteoporosis, cancer, glaucoma, epilepsy, and obesity. Because of these critical physiological functions, extensive studies have been conducted on CAs and CAIs. Among the isoenzymes, CA I and CA II have received the most comprehensive examination. The data in Table 1 demonstrate that the 1,4-naphthoquinone thiazole hybrids (**3a–e**) showed moderate inhibitory effects against the *h*CA I isoform. Studied compounds demonstrated potent inhibition of the *h*CA I isoform at nanomolar levels, with K_I values spanning from 67.86 ± 8.06 to 161.60 ± 20.19 nM. Comparatively, AAZ, a CA inhibitor with broad specificity, exhibited a K_I value of 20.52 ± 3.17 nM against *h*CA I. In set of compounds (**3a–e**), the most active compound was **3d** with a K_I value of 67.86 nM for *h*CA I (Fig. 3). The potency of studied compound indicated the following order for *h*CA I **3d** (K_I: 67.86±8.06 nM) > **3e** (K_I: 85.14±9.39 nM) > **3b** (K_I: 109.90 ±13.03 nM) > **3a** (K_I: 142.30±16.32 nM) > **3c** (K_I: 161.60±20.19 nM). The 4-chlorophenyl (**3d**) group exhibited 1.90 times more inhibition effect on *h*CA I inhibition than the 4-fluorophenyl group (**3c**). Additionally, the 4-methoxyphenyl (**3b**) group exhibited 1.29 times less inhibition effect on *h*CA I inhibition than the 4-bromophenyl (**3e**) group. In other words, bromine was more effective in terms of inhibition than the methoxy group.

These new1,4-naphthoquinone thiazole hybrids (**3a–e**) demonstrated a notable degree of inhibition against *h*CA II. Additionally, AAZ showed a K_I value of 23.77 ± 4.01 nM against *h*CA II. Notably, compounds **3b** and **3d** displayed the most significant inhibitory effects, with K_I values of 55.27 ± 5.92 and 56.85 ± 6.79 nM, respectively. Considering this result, 4-methoxyphenyl group and 4-chlorophenyl group inhibited the *h*CA II enzyme at almost the same level. When sorted according to the inhibition effect of the connected groups, it is as follows: 4-methoxyphenyl > 4-chlorophenyl > 4-fluorophenyl > 4-phenyl > 4-bromophenyl. In contrast to *h*CA I, *h*CA II showed the least inhibition compared to the others, with the 4-bromophenyl linked compound (**3e**).

ii) The inhibition properties of 1,4-naphthoquinone thiazole hybrids (**3a–e**) on AChE and BChE were assessed using Ellman's procedure [57], as previously described. These derivatives proved to be potent, with K_I values ranging from 26.12 to 98.42 nM for AChE (Table 1) and 45.03 to 84.43 nM for BChE. In contrast, THA exhibited K_I values of 81.21 nM against AChE and 73.13 nM against BChE. All the studied compounds demonstrated strong inhibition of the cholinergic enzyme AChE, with **3e** displaying the most effective inhibition. The potency of studied compound indicated the following order for AChE **3e** (K_I: 26.12±2.54 nM) > **3e** (K_I: 27.46±2.86 nM) > **3c** (K_I: 73.57±6.11 nM) > **3a** (K_I: 85.57±7.50 nM) > **3d** (K_I: 98.42±8.70 nM). The 4-chlorophenyl (**3d**) group exhibited 1.34 times less inhibition effect on AChE inhibition than the 4-fluorophenyl group (**3c**). Additionally, the 4-methoxyphenyl (**3b**) group exhibited 3.28 times less inhibition effect on AChE inhibition than the 4-bromophenyl (**3e**) group.

On the contrary, when assessing the inhibition results for BChE, it was apparent that **3c** emerged as the most effective inhibitor, boasting a K_I value of 45.03 nM, which is 1.69 times lower than THA (K_I: 73.13 nM). When sorted according to the inhibition effect of the connected groups, it is as follows: 4-fluorophenyl > 4-methoxyphenyl > 4-phenyl > 4-chlorophenyl > 4-bromophenyl. The 4-fluorophenyl (**3c**) group

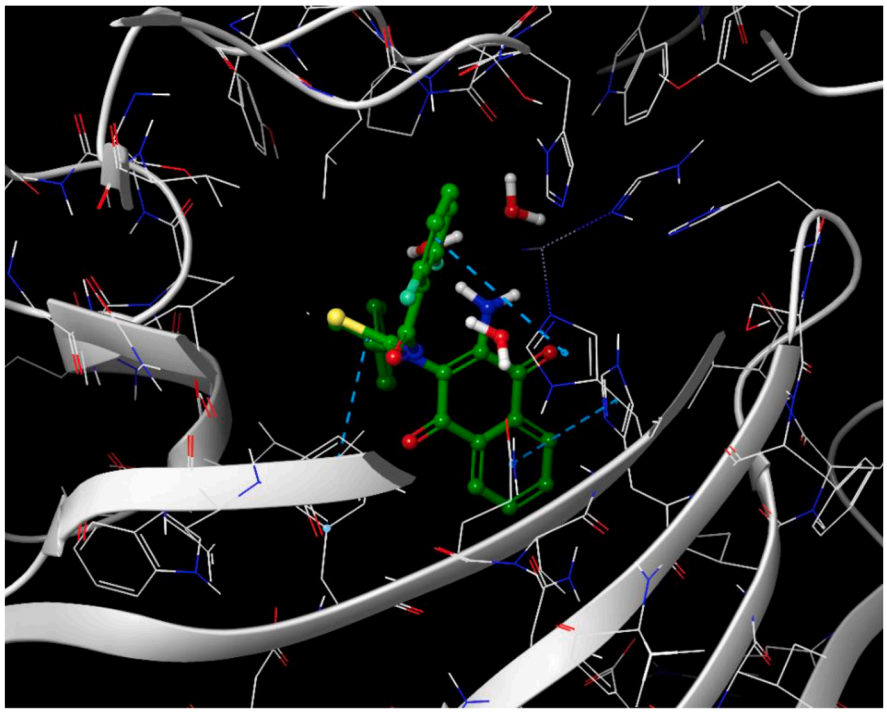

A

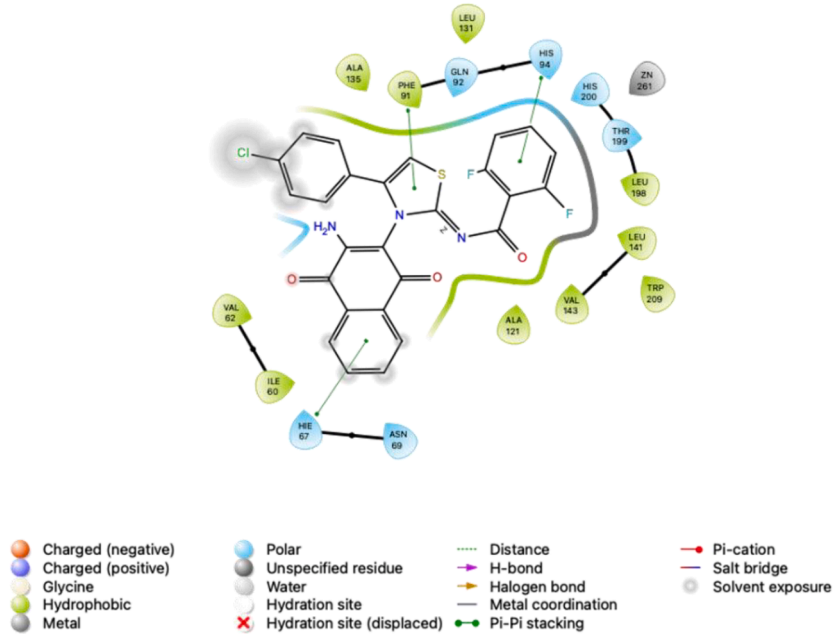

B

Fig. 4. The *h*CA I isoform (PDB ID 1AZM) was subjected to molecular docking with *N*-[3-(3-amino-1,4-dioxo-1,4-dihydronaphthalen-2-yl)-4-(4-chlorophenyl)thiazol-2(3*H*)-ylidene]-2,6-difluorobenzamide (**3d**), which yielded the 3D docking pose of the compound **3d** within the binding pocket of 1AZM (depicted in **A**). Further, the 2D interaction diagram (depicted in **B**) was generated to elucidate the interactions of 1AZM with compound **3d**

exhibited 1.54 times more inhibition effect on BChE inhibition than the 4-chlorophenyl group (**3d**).

3.3. Computational study

The efficacy of the Glide XP docking protocol was assessed by re-docking the co-crystallized native ligands, namely 5-acetamido-1,3,4-thiadiazole-2-sulfonamide (*h*CAs with AZM/AAZ) and 1,2,3,4-tetrahydroacridin-9-amine (ChEs with THA), into the active sites of these enzymes (PDB IDs 1AZM [61] and 3HS4 [63] for *h*CA I and *h*CA II, and 7XN1 [65] and 4BDS [67] for AChE and BChE, respectively) using Small-Molecule Drug Discovery Suite 2023-3 for Mac. The root mean

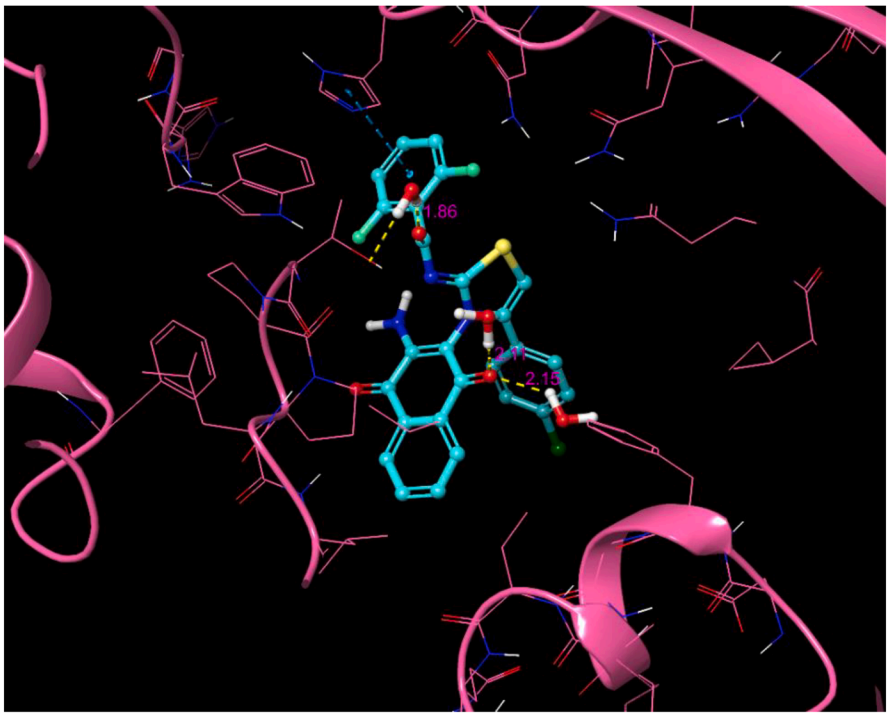

A

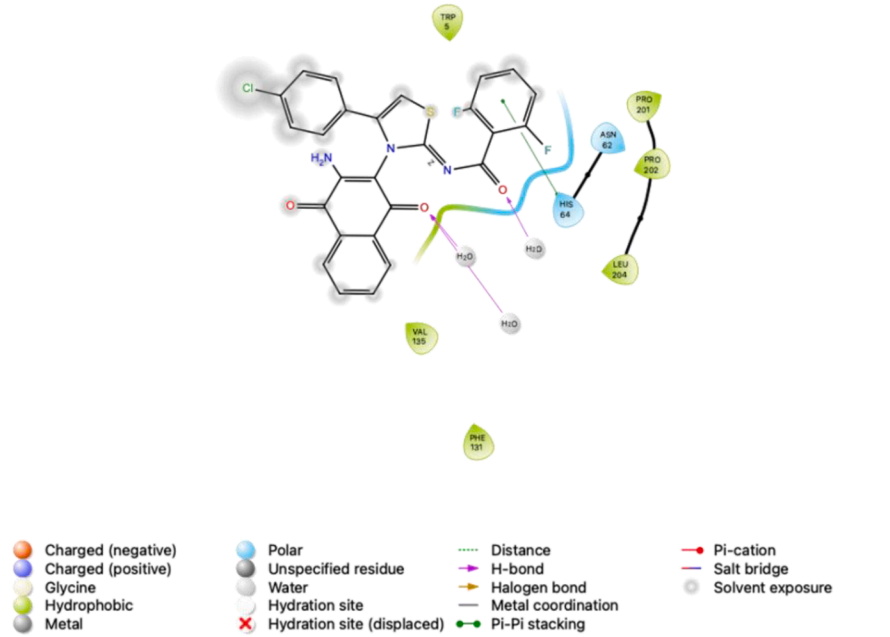

B

Fig. 5. The *h*CA II isoform (PDB ID 3HS4) was subjected to molecular docking with *N*-[3-(3-amino-1,4-dioxo-1,4-dihydronaphthalen-2-yl)-4-(4-chlorophenyl)thiazol-2(3*H*)-ylidene]-2,6-difluorobenzamide (**3d**), which yielded the 3D docking pose of the compound **3d** within the binding pocket of 3HS4 (depicted in **A**). Further, the 2D interaction diagram (depicted in **B**) was generated to elucidate the interactions of 3HS4 with compound **3d**

square deviation values between the conformation of the native ligands (AAZ and THA) and the optimal pose generated by this protocol were found to be 0.15, 1.41, 0.04, and 0.03 Å, respectively. These results indicated that the Glide XP docking algorithm is suitable for docking new 1,4-naphthoquinone thiazole hybrids (**3a–e**) to the active pockets of the *h*CAs and ChEs enzymes. Figs. 4–7 exemplify that the docking scores of **3d** (for both *h*CA), **3e**, and **3c**, namely −4.26 kcal/mol for *h*CA I, −3.43 kcal/mol for *h*CA II, −6.94 kcal/mol for AChE, and −9.70 kcal/mol for BChE, demonstrate comparable conformations. Specifically, these conformations involve interactions such as H-bond and π-π stacking within the respective enzyme-binding pockets.

Herein, the naphthalene, thiazole, and difluorobenzene rings

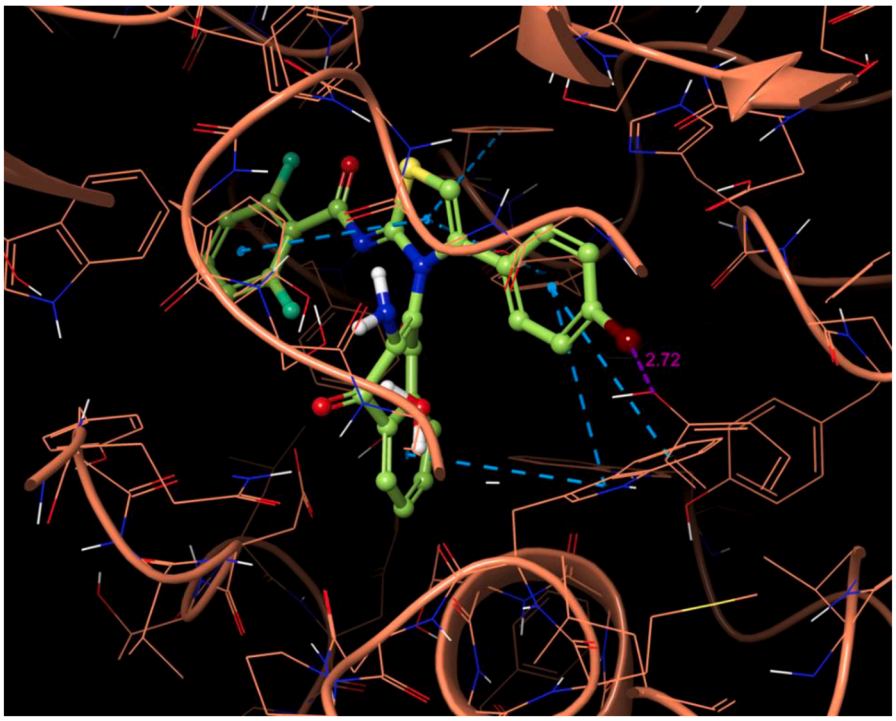

A

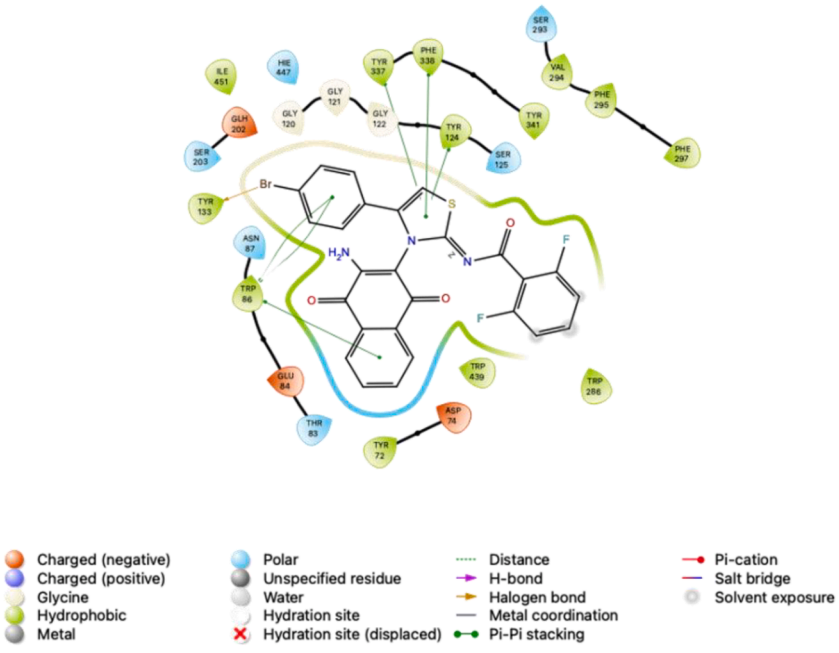

B

Fig. 6. The AChE (PDB ID 7XN1) was subjected to molecular docking with *N*-[3-(3-amino-1,4-dioxo-1,4-dihydronaphthalen-2-yl)-4-(4-bromophenyl)thiazol-2(3*H*)-ylidene]-2,6-difluorobenzamide (**3e**), which yielded the 3D docking pose of the compound **3e** within the binding pocket of 7XN1 (depicted in **A**). Further, the 2D interaction diagram (depicted in **B**) was generated to elucidate the interactions of 7XN1 with compound **3e**.

engaged in π-π stacking with the residues His67, Phe91, and His94, respectively, in *h*CA I. The *h*CA II interacted by H-bond with the carbonyl groups (in distances 1.86, 2.11. and 2.15 Å) as well as π-π stacking between His64 and difluorobenzene ring. The AChE formed an H-bond interaction between the bromine of the bromobenzene ring and Tyr133 residue (2.72 Å) and π-π stacking between naphthalene, thiazole, and difluorobenzene rings and hydrophobic residues Trp86, Tyr124, Tyr337, and Phe338. The carbonyl groups engaged in H-bond with the Gly116 (2.25 Å) and a water molecule (1.64 Å) in BChE, while additionally, H-bond was exhibited between Gly116 (2.43 Å) and a water molecule. Additionally, the Trp82 and His438 residues formed π-π stacking interactions with the fluorobenzene and thiazole ring

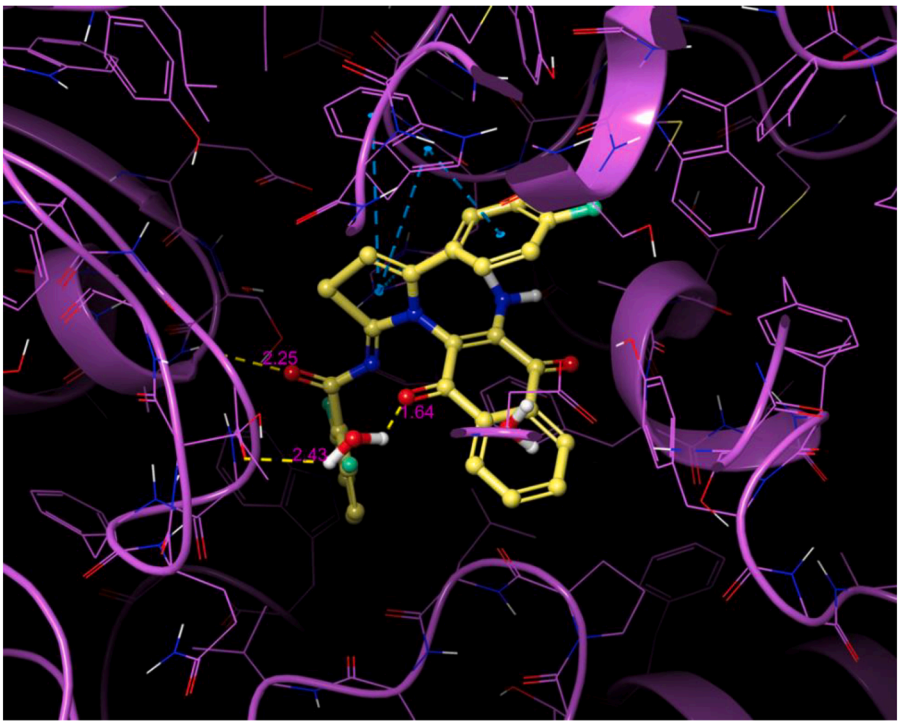

A

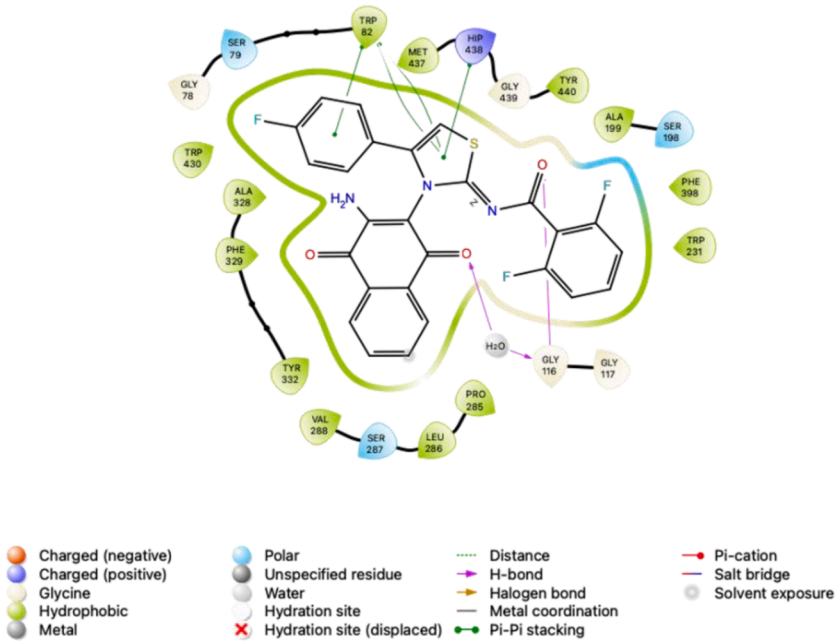

B

Fig. 7. The BChE (PDB ID 4BDS) was subjected to molecular docking with *N*-[3-(3-amino-1,4-dioxo-1,4-dihydronaphthalen-2-yl)-4-(4-fluorophenyl)thiazol-2(3*H*)-ylidene]-2,6-difluorobenzamide (**3c**), which yielded the 3D docking pose of the compound **3c** within the binding pocket of 4BDS (depicted in **A**). Further, the 2D interaction diagram (depicted in **B**) was generated to elucidate the interactions of 4BDS with compound **3c**.

(Figs. 4–7).

These molecular docking results ensured insights into the ligand-protein interactions. It rationalized the experimental data and confirmed that the binding modes of the most active derivatives in series (**3d, 3e**, and **3d**) against *h*CAs and ChEs have the most favorable binding free energy.

Moreover, the 1,4-naphthoquinone thiazole hybrids (**3a–e**) were assessed for their drug-like properties utilizing the QikProp module of the Schrödinger Suite 2023-3 for Mac. The chosen ADME/T parameters were calculated and documented in Table 2. The molecular weights (MWs, 487.5 - 566.4) and dipole moments (Dipole, in the 6.8 to 9.2) of new synthesized 1,4-naphthoquinone thiazole hybrids **3a–e** have

Table 2
ADME/T related parameters [a] of new synthesized 1,4-naphthoquinone thiazole hybrids **3a–e** and the reference inhibitors acetazolamide and tacrine.

Compounds ID	CNS	MW	Dipole	Volume	donorHB	acceptHB	QPlogPoct	QPlogPw	QPlogPo/w	QPlogS	QPlogHERG	QPPCaco	QPlogBB	QPlogKp	Metab	QPlogKhsa	HOA	PSA	Rule of Five	Rule of Three
3a	–1	487.5	8.3	1344.7	1.5	8.0	24.7	15.0	4.4	–6.5	–7.1	601.5	–0.7	–1.8	2	0.5	100.0	110.2	0	1
3b	–1	517.5	9.2	1421.6	1.5	8.8	25.8	15.2	4.5	–6.7	–7.0	593.2	–0.8	–1.9	3	0.5	90.0	118.5	1	1
3c	–1	505.5	6.8	1360.6	1.5	8.0	24.8	14.7	4.7	–6.8	–6.9	603.0	–0.6	–1.9	2	0.6	91.0	110.1	1	1
3d	–1	521.9	6.9	1388.3	1.5	8.0	25.2	14.7	4.9	–7.2	–7.0	602.3	–0.6	–1.9	2	0.6	92.5	110.1	1	1
3e	–1	566.4	7.0	1397.6	1.5	8.0	25.4	14.7	5.0	–7.3	–7.0	601.9	–0.6	–1.9	2	0.6	92.9	110.1	1	1
AAZ [b]	–2	222.2	10.9	634.3	3.0	9.0	17.6	15.2	–1.8	–1.6	–3.8	35.5	–1.8	–5.9	1	–1.0	44.4	133.3	0	0
THA [c]	1	198.3	4.2	710.0	1.5	2.0	10.7	6.4	2.6	–3.1	–4.2	2931.3	0.1	–1.8	3	0.1	100.0	34.2	0	0

[a] CNS, Central nervous system activity (–2 inactive, +2 active); MW, molecular weight of the compound (130.0 - 725.0); Dipole, computed dipole moment of the compound (1.0 - 12.5); Volume, total solvent-accessible volume in cubic angstroms using a probe with a 1.4 Å Radius (500.0 - 2000.0); donorHB, estimated number of hydrogen bonds that would be donated by the solute to water molecules in an aqueous solution (0.0 - 6.0); acceptHB, estimated number of hydrogen bonds that would be accepted by the solute from water molecules in an aqueous solution (2.0 – 20.0); QPlogPoct, octanol/gas partition coefficient (8.0 - 35.0); QPlogPw, water/gas partition coefficient (4.0 - 45.0); QPlogPo/w, octanol/water partition coefficient (–2.0 - 6.5); QPlogS, aqueous solubility (–6.5 - 0.5); QPlogHERG, IC_{50} value for blockage of HERG K^+ channels (concern below –5); QPPCaco, apparent Caco-2 cell permeability in nm/sec (<25 poor, great>500); QPlogBB, brain/blood partition coefficient (–3.0 - 1.2); QPlogKp, skin permeability (–8.0 - –1.0); Metab, number of likely metabolic reactions (1 - 8); QPlogKhsa, prediction of binding to human serum albumin (–1.5 - 1.5); HOA; human oral absorption (<25% poor, high>80%); PSA, van der Waals surface area of polar nitrogen and oxygen atoms (7.0 - 200.0); Rule of Five, number of violations of Lipinski's rule of five (max. 4); and Rule of Three, number of violations of Jorgensen's rule of three (max. 2).

[b] Acetazolamide.

[c] Tacrine.

Table 3
pK_a values of **3a–e** 25% (*v/v*) DMSO:water, 25.0 ± 0.1 °C, I = 0.1 M NaCl.

	3a	3b	3c	3d	3e
pK_{a1}	2.62±0.01	2.60±0.03	2.90±0.03	2.50±0.02	2.60±0.03
pK_{a2}	6.75±0.01	6.78±0.03	6.79±0.04	6.80±0.02	6.76±0.03
pK_{a3}	10.88±0.01	10.75±0.03	10.96±0.04	10.73±0.02	10.84±0.04

reported being in the permissible values. Volume (in range 1344.7 to 1397.6), the total solvent-accessible volume descriptor, was determined to be in the allowable ranges for these target compounds (**3a–e**), compared with reference values. The log P values, such as QPlogPoct, QPlogPw, QPlogPo/w, QPlogS, QPlogHERG, QPlogBB, QPlogKp, and QPlogKhs, are in ranging from 24.7 to 25.8, 14.7 to 15.2, 4.4 to 5.0, –7.3 to –6.5, –7.1 to –6.9, –0.8 to –0.6, –1.9 to –1.8, and 0.5 to 0.6, respectively, indicate of these molecules (3a-e) have a high capacity. The values of human oral absorption (HOAs) range between 90.0% and 100.0%, and the van der Waals surface area of polar nitrogen and oxygen atoms (PSA, in the range 110.1 to 118.5), indicating that all derivatives (**3a–e**) had at the acceptable values. All the products have displayed high Caco-2 cell permeability rates (593.2 to 603.0). These findings indicated that, based on their physicochemical attributes, the derivatives **3a–e** fulfilled the criteria for drug-like molecules as stipulated by Lipinski's [91] and Jorgensen's [92] guidelines.

3.4. Acid dissociation constants

The pK_a value is one of the critically important physicochemical parameters which provide information about acidity, basicity, solubility, hydrogen bond capacity and other many properties [90]. While doing drug design studies, knowing the pK_a value(s) of the compound in advance can prevent many unnecessary costs and loss of time. Since most drug molecules have one or more ionizable groups and are active in the living system in the ionized form, it is important to know the pK_a value, which provides information about the concentration of the ionized forms of the compound in its environment [93]. For this reason, we carried out studies to determine the pK_a values of **3a–e** that showed significant enzyme inhibition properties. The pK_a values of **3a–e** were calculated by HYPERQUAD computer program using the data obtained from potentiometric titrations. The pK_a values of **3a–e** ligands are given in Table 3, and titration curves of **3a–e** and the distribution curve of **3a** for symbolizing all **3a–e** ligands are presented in Fig. 8A and B, respectively. Distribution curves of **3b–e** ligands are presented in supplementary material (Fig. S21).

Three pK_a values for **3a–e** could be determined in the experimental conditions performed and the pK_{a1}, pK_{a2}, and pK_{a3} values were found in a range of 2.50±0.02 – 2.90±0.03, 6.75±0.01 – 6.80±0.02, and 10.73 ±0.02–10.96±0.04, respectively (Table 3). Altun et al. reported that the pK_a of *N*-(thiazol-2-yl)methanimine scaffold is in the range of 2.46–2.85 [94], while Öğretir et al. [95] reported that the pK_a value of the nitrogen atom of thiazoles in the imino form ranged from 4.16 to 3.36. Like aromatic amines such as aniline (pK_a= 1.02–6.08), which are known to show acidic character, the NH_2 group of the naphthoquinone scaffold is expected to show an acidic character [96]. 1,4-naphthoquinones, which behave like naphthalene-1,4-diol due to delocalization, are expected to display basic character and generally have a pK_a value above 10 in the DMSO:water mixture [36,37]. According to literature information, it is possible to say that the pK_{a1}, pK_{a2}, and pK_{a3} calculated for the DMSO: water medium mentioned above may be related to protonated imino nitrogen, amine, and carbonyl oxygen atom of naphthoquinone scaffold, respectively.

4. Conclusion

In summary, we have demonstrated that starting from molecule **2**, the cyclization products resulting from the reaction with

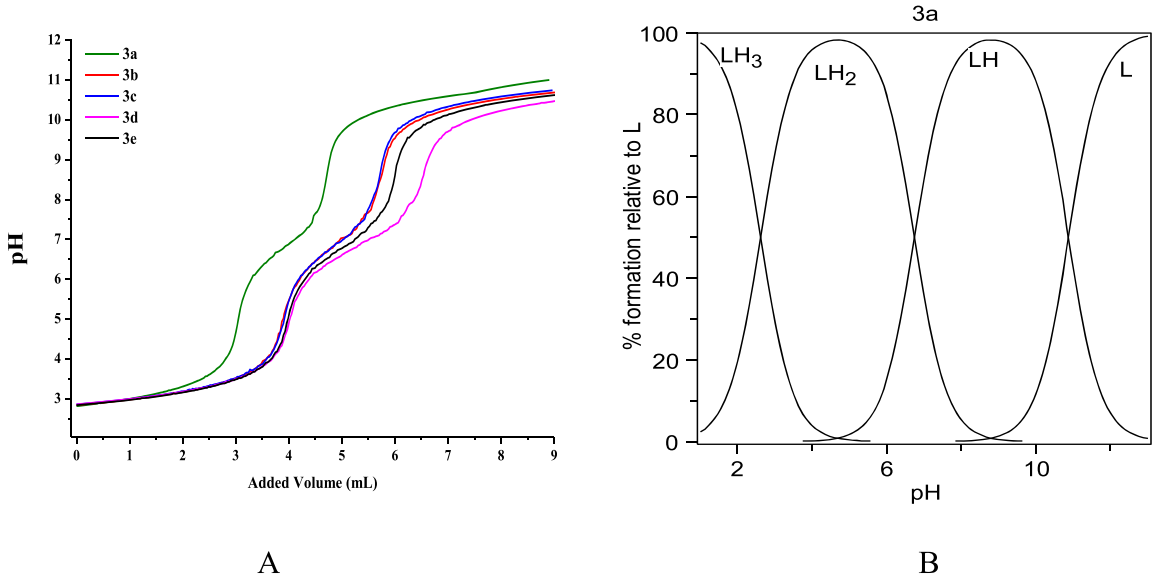

Fig. 8. A) Titration curves of **3a–e** (25.0 ± 0.1 °C, I = 0.1 M NaCl, DMSO:water 25:75 *v/v*). B) Distribution curve of **3a**.

α-bromoketones of new thiazole naphthoquinone hybrids bearing 2,6-difluorophenyl **3a–e** were synthesized. X-ray diffraction analysis of *N*-[3-(3-amino-1,4-dioxo-1,4-dihydronaphthalen-2-yl)-4-phenylthiazol-2(3*H*)-ylidene]-2,6-difluorobenzamide **3a** was performed. Determination of this structure provided certainty for other structures. The study involved the evaluation of the inhibitory effects of several new thiazole naphthoquinone hybrids bearing 2,6-difluorophenyl **3a–e** on *h*CA I, and II isoenzymes, as well as AChE and BChE. These compounds used in our research demonstrated significant inhibition of studied enzymes activities at low nanomolar concentrations. Additionally, molecular docking was employed to examine the binding of novel thiazole hybrids of naphthoquinone to the active sites of *h*CAs and ChEs. The findings indicate that these compounds (**3a–e**) align favorably with the active sites of these enzymes. Moreover, it has been determined that these compounds being investigated exhibit drug-like characteristics based on their physicochemical properties, and all of the derivatives (**3a–e**) adhere to the guidelines established by Lipinski and Jorgensen. These findings suggest that these compounds hold promise for the development of new CA isoenzyme and cholinesterase inhibitors and drugs for the treatment of specific diseases.

CRediT authorship contribution statement

Cagla Efeoglu: Formal analysis, Investigation, Methodology. **Ozge Selcuk:** Formal analysis, Investigation, Methodology. **Bunyamin Demir:** Formal analysis, Investigation, Methodology. **Ertan Sahin:** Conceptualization, Formal analysis, Investigation, Methodology, Writing – original draft. **Hayati Sari:** Conceptualization, Formal analysis, Investigation, Methodology, Writing – original draft. **Cüneyt Türkeş:** Conceptualization, Data curation, Formal analysis, Investigation, Methodology, Writing – original draft, Writing – review & editing. **Yeliz Demir:** Conceptualization, Data curation, Formal analysis, Investigation, Methodology, Writing – original draft, Writing – review & editing, Supervision. **Yahya Nural:** Conceptualization, Data curation, Formal analysis, Funding acquisition, Investigation, Methodology, Project administration, Supervision, Writing – original draft, Writing – review & editing. **Şükrü Beydemir:** Conceptualization, Data curation, Formal analysis, Investigation, Methodology, Writing – original draft, Writing – review & editing.

Declaration of Competing Interest

The authors declare that they have no known competing financial interests or personal relationships that could have appeared to influence the work reported in this paper.

Data availability

No data was used for the research described in the article.

Acknowledgments

We are thankful to the Scientific and Technological Research Council of Turkey (TÜBİTAK, project grant 118Z407) and the Research Fund of Anadolu University (grant number 2102S003) for the financial support.

Supplementary materials

Supplementary material associated with this article can be found, in the online version, at doi:10.1016/j.molstruc.2023.137365.

References

[1] M. Gümüş, Ş.N. Babacan, Y. Demir, Y. Sert, İ. Koca, İ. Gülçin, Discovery of sulfadrug–pyrrole conjugates as carbonic anhydrase and acetylcholinesterase inhibitors, Arch. Pharm. (Weinheim) 355 (2022), https://doi.org/10.1002/ardp.202100242.

[2] M. Boztaş, Y. Çetinkaya, M. Topal, İ. Gülçin, A. Menzek, E. Şahin, M. Tanc, C. T. Supuran, Synthesis and carbonic anhydrase isoenzymes I, II, IX, and XII inhibitory effects of dimethoxybromophenol derivatives incorporating cyclopropane moieties, J. Med. Chem. 58 (2015) 640–650, https://doi.org/10.1021/jm501573b.

[3] P. Taslimi, H.E. Aslan, Y. Demir, N. Oztaskin, A. Maraş, İ. Gulçin, S. Beydemir, S. Goksu, Diarylmethanon, bromophenol and diarylmethane compounds: discovery of potent aldose reductase, α-amylase and α-glycosidase inhibitors as new therapeutic approach in diabetes and functional hyperglycemia, Int. J. Biol. Macromol. 119 (2018) 857–863, https://doi.org/10.1016/j.ijbiomac.2018.08.004.

[4] M. Hamide, Y. Gök, Y. Demir, G. Yakalı, T.T. Tok, A. Aktaş, R. Sevinçek, B. Güzel, İ. Gülçin, Pentafluorobenzyl-substituted benzimidazolium salts: synthesis, characterization, crystal structures, computational studies and inhibitory properties of some metabolic enzymes, J. Mol. Struct. 1265 (2022), 133266, https://doi.org/10.1016/j.molstruc.2022.133266.

[5] Ö. Demirci, B. Tezcan, Y. Demir, T. Taskin-Tok, Y. Gök, A. Aktaş, B. Güzel, İ. Gülçin, Acetylphenyl-substituted imidazolium salts: synthesis, characterization, *in silico* studies and inhibitory properties against some metabolic enzymes, Mol. Divers. (2022), https://doi.org/10.1007/s11030-022-10578-3.

[6] A. Cetin, E. Bursal, F. Türkan, 2-methylindole analogs as cholinesterases and glutathione S-transferase inhibitors: synthesis, biological evaluation, molecular docking, and pharmacokinetic studies: 2-methylindole analogs as cholinesterases and glutathione S-transferase inhibitors, Arab. J. Chem. 14 (2021), https://doi.org/10.1016/j.arabjc.2021.103449.

[7] A. Cetin, F. Türkan, E. Bursal, M. Murahari, Synthesis, characterization, enzyme inhibitory activity, and molecular docking analysis of a new series of thiophene-based heterocyclic compounds, Russ. J. Org. Chem. 57 (2021), https://doi.org/10.1134/S107042802104014X.

[8] Y. Chen, M. Dang, Z. Zhang, Brain mechanisms underlying neuropsychiatric symptoms in Alzheimer's disease: a systematic review of symptom-general and –specific lesion patterns, Mol. Neurodegener. 16 (2021) 38, https://doi.org/10.1186/s13024-021-00456-1.

[9] B. Dubois, H. Hampel, H.H. Feldman, P. Scheltens, P. Aisen, S. Andrieu, H. Bakardjian, H. Benali, L. Bertram, K. Blennow, K. Broich, E. Cavedo, S. Crutch, J. Dartigues, C. Duyckaerts, S. Epelbaum, G.B. Frisoni, S. Gauthier, R. Genthon, A. A. Gouw, M. Habert, D.M. Holtzman, M. Kivipelto, S. Lista, J. Molinuevo, S. E. O'Bryant, G.D. Rabinovici, C. Rowe, S. Salloway, L.S. Schneider, R. Sperling, M. Teichmann, M.C. Carrillo, J. Cummings, C.R. Jack, Preclinical Alzheimer's disease: definition, natural history, and diagnostic criteria, Alzheimer. Dement. 12 (2016) 292–323, https://doi.org/10.1016/j.jalz.2016.02.002.

[10] F. Türkan, Z. Huyut, Y. Demir, F. Ertaş, Ş. Beydemir, The effects of some cephalosporins on acetylcholinesterase and glutathione S-transferase: an *in vivo* and *in vitro* study, Arch. Physiol. Biochem. 125 (2019) 235–243, https://doi.org/10.1080/13813455.2018.1452037.

[11] S. Jokar, S. Khazaei, H. Behnammanesh, A. Shamloo, M. Erfani, D. Beiki, O. Bavi, Recent advances in the design and applications of amyloid-β peptide aggregation inhibitors for Alzheimer's disease therapy, Biophys. Rev. 11 (2019) 901–925, https://doi.org/10.1007/s12551-019-00606-2.

[12] N.A.-E. El-Sayed, A.E.-S. Farag, M.A.F. Ezzat, H. Akincioglu, İ. Gülçin, S.M. Abou-Seri, Design, synthesis, *in vitro* and *in vivo* evaluation of novel pyrrolizine-based compounds with potential activity as cholinesterase inhibitors and anti-Alzheimer's agents, Bioorg. Chem. 93 (2019), 103312, https://doi.org/10.1016/j.bioorg.2019.103312.

[13] C. Caglayan, Y. Demir, S. Kucukler, P. Taslimi, F.M. Kandemir, İ. Gulçin, The effects of hesperidin on sodium arsenite-induced different organ toxicity in rats on metabolic enzymes as antidiabetic and anticholinergics potentials: a biochemical approach, J. Food Biochem. 43 (2019) e12720, https://doi.org/10.1111/jfbc.12720.

[14] A. Singh, D. Malhotra, K. Singh, R. Chadha, P.M.S. Bedi, Thiazole derivatives in medicinal chemistry: recent advancements in synthetic strategies, structure activity relationship and pharmacological outcomes, J. Mol. Struct. 1266 (2022), 133479, https://doi.org/10.1016/j.molstruc.2022.133479.

[15] P. Mohanty, S. Behera, R. Behura, L. Shubhadarshinee, P. Mohapatra, A.K. Barick, B.R. Jali, Antibacterial activity of thiazole and its derivatives: a review, Biointerface Res. Appl. Chem. 12 (2021) 2171–2195, https://doi.org/10.33263/BRIAC122.21712195.

[16] S. Murru, C.B. Singh, V. Kavala, B.K. Patel, A convenient one-pot synthesis of thiazol-2-imines: application in the construction of pifithrin analogues, Tetrahedron 64 (2008) 1931–1942, https://doi.org/10.1016/j.tet.2007.11.076.

[17] A.M. Abdallah, S.M. Gomha, M.E.A. Zaki, T.Z. Abolibda, N.A. Kheder, A green synthesis, DFT calculations, and molecular docking study of some new indeno[2,1-*b*]quinoxalines containing thiazole moiety, J. Mol. Struct. 1292 (2023), 136044, https://doi.org/10.1016/j.molstruc.2023.136044.

[18] A.A. Alia, A. Alharbi, J. Qurban, M.M. Abualnaja, H.M. Abumelha, F.A. Saad, N. M. El-Metwaly, Molecular modeling and docking studies of new antioxidant pyrazole-thiazole hybrids, J. Mol. Struct. 1267 (2022), 133582, https://doi.org/10.1016/j.molstruc.2022.133582.

[19] A. Doğan, S. Özdemir, M.S. Yalçın, H. Sarı, Y. Nural, Naphthoquinone–thiazole hybrids bearing adamantane: synthesis, antimicrobial, DNA cleavage, antioxidant activity, acid dissociation constant, and drug-likeness, J. Res. Pharm. 25 (3) (2021) 292–304, https://doi.org/10.29228/jrp.20.

[20] N.V. Sadgir, V.A. Adole, S.L. Dhonnar, B.S. Jagdale, Synthesis and biological evaluation of coumarin appended thiazole hybrid heterocycles: antibacterial and antifungal study, J. Mol. Struct. 1293 (2023), 136229, https://doi.org/10.1016/J.MOLSTRUC.2023.136229.

[21] E.A. Hassan, S.E. Zayed, A.-H.S. Mahdy, A.M. Abo-Bakr, An efficient protocol for the synthesis of new camphor pyrimidine and camphor thiazole derivatives using conventional and microwave irradiation techniques and *in vitro* evaluation as potential antimicrobial agents, Curr. Org. Synth. 19 (2022) 558–568, https://doi.org/10.2174/1570179419666220104125340.

[22] Y. Nural, Synthesis, antimycobacterial activity, and acid dissociation constants of polyfunctionalized 3-[2-(*pyrrolidin*-1-*yl*)*thiazole*-5-*carbonyl*]-2H-chromen-2-one derivatives, Monatshefte Für Chemie - Chem. Month. 149 (2018) 1905–1918, https://doi.org/10.1007/s00706-018-2250-7.

[23] Y. Nural, M. Gemili, M. Ulger, H. Sari, L.M. De Coen, E. Sahin, Synthesis, antimicrobial activity and acid dissociation constants of methyl 5,5-diphenyl-1-(thiazol-2-yl)pyrrolidine-2-carboxylate derivatives, Bioorg. Med. Chem. Lett. 28 (2018) 942–946, https://doi.org/10.1016/j.bmcl.2018.01.045.

[24] R.H.H. Salih, A.H. Hasan, N.H. Hussen, F.E. Hawaiz, T. Ben Hadda, J. Jamalis, F. A. Almalki, A.S. Adeyinka, L.-C.C. Coetzee, A.K. Oyebamiji, Thiazole-pyrazoline hybrids as potential antimicrobial agent: synthesis, biological evaluation, molecular docking, DFT studies and POM analysis, J. Mol. Struct. 1282 (2023), 135191, https://doi.org/10.1016/j.molstruc.2023.135191.

[25] Y. Nural, M. Gemili, E. Yabalak, L.M. De Coen, M. Ulger, Green synthesis of highly functionalized octahydropyrrolo[3,4-*c*]pyrrole derivatives using subcritical water, and their anti(myco)bacterial and antifungal activity, Arkivoc 2018 (2018) 51–64, https://doi.org/10.24820/ark.5550190.p010.573.

[26] R. Palabindela, R. Guda, G. Ramesh, R. Bodapati, S.K. Nukala, P. Myadaraveni, G. Ravi, M. Kasula, Curcumin based pyrazole-thiazole hybrids as antiproliferative agents: synthesis, pharmacokinetic, photophysical properties, and docking studies, J. Mol. Struct. 1275 (2023), 134633, https://doi.org/10.1016/J.MOLSTRUC.2022.134633.

[27] M. Fan, Q. Feng, W. Yang, Z. Peng, G. Wang, Thiazole-benzamide derivatives as α-glucosidase inhibitors: synthesis, kinetics study, molecular docking, and *in vivo* evaluation, J. Mol. Struct. 1291 (2023), 136011, https://doi.org/10.1016/J.MOLSTRUC.2023.136011.

[28] M. Taha, S. Hayat, F. Rahim, N. Uddin, A. Wadood, M. Nawaz, M. Gollapalli, A. U. Rehman, K.M. Khan, R.K. Farooq, Exploring thiazole-based Schiff base analogs as potent α-glucosidase and α-amylase inhibitor: their synthesis and *in-silico* study, J. Mol. Struct. 1287 (2023), 135672, https://doi.org/10.1016/J.MOLSTRUC.2023.135672.

[29] S. Mor, M. Khatri, Synthesis, antimicrobial evaluation, α-amylase inhibitory ability and molecular docking studies of 3-alkyl-1-(4-(aryl/heteroaryl)thiazol-2-yl)indeno[1,2-*c*]pyrazol-4(1H)-ones, J. Mol. Struct. 1249 (2022), 131526, https://doi.org/10.1016/j.molstruc.2021.131526.

[30] B. Sever, C. Türkeş, M.D. Altıntop, Y. Demir, G. Akalın Çiftçi, Ş. Beydemir, Novel metabolic enzyme inhibitors designed through the molecular hybridization of thiazole and pyrazoline scaffolds, Arch. Pharm. (Weinheim) 354 (2021), 2100294, https://doi.org/10.1002/ardp.202100294.

[31] E.C. Erigür, C. Altuğ, A. Angeli, C.T. Supuran, Design, synthesis and human carbonic anhydrase I, II, IX and XII inhibitory properties of 1,3-thiazole sulfonamides, Bioorg. Med. Chem. Lett. 59 (2022), 128581, https://doi.org/10.1016/j.bmcl.2022.128581.

[32] S. Khan, H. Ullah, M. Taha, F. Rahim, M. Sarfraz, R. Iqbal, N. Iqbal, R. Hussain, S. A. Ali Shah, K. Ayub, M.A. Albalawi, M.A. Abdelaziz, F.S. Alatawi, K.M. Khan, Synthesis, DFT studies, molecular docking and biological activity evaluation of thiazole-sulfonamide derivatives as potent Alzheimer's inhibitors, Molecules 28 (2023) 559, https://doi.org/10.3390/molecules28020559.

[33] R. Hussain, H. Ullah, F. Rahim, M. Sarfraz, M. Taha, R. Iqbal, W. Rehman, S. Khan, S.A.A. Shah, S. Hyder, M. Alhomrani, A.S. Alamri, O. Abdulaziz, M.A. Abdelaziz, Multipotent cholinesterase inhibitors for the treatment of Alzheimer's disease: synthesis, biological analysis and molecular docking study of benzimidazole-based thiazole derivatives, Molecules 27 (2022) 6087, https://doi.org/10.3390/MOLECULES27186087/S1.

[34] M. Devi, P. Kumar, R. Singh, L. Narayan, A. Kumar, J. Sindhu, S. Lal, K. Hussain, D. Singh, A comprehensive review on synthesis, biological profile and photophysical studies of heterocyclic compounds derived from 2,3-diamino-1,4-naphthoquinone, J. Mol. Struct. 1269 (2022), 133786, https://doi.org/10.1016/J.MOLSTRUC.2022.133786.

[35] C. Efeoglu, D. Yetkin, Y. Nural, A. Ece, Z. Seferoğlu, F. Ayaz, Novel urea-thiourea hybrids bearing 1,4-naphthoquinone moiety: anti-inflammatory activity on mammalian macrophages by regulating intracellular PI3K pathway, and molecular docking study, J. Mol. Struct. 1264 (2022), 133284, https://doi.org/10.1016/J.MOLSTRUC.2022.133284.

[36] C. Canatar, H. Türkben, C. Efeoglu, H. Sari, E. Karasu, Y. Nural, F. Ayaz, Anti-inflammatory potential of 1,4-naphthoquinone acyl thiourea hybrids on lipopolysaccharide-activated mammalian macrophages, and their acid dissociation constants, ChemistrySelect 8 (2023), e202301258, https://doi.org/10.1002/slct.202301258.

[37] Y. Nural, S. Ozdemir, O. Doluca, B. Demir, M.S. Yalcin, H. Atabey, B. Kanat, S. Erat, H. Sari, Z. Seferoglu, Synthesis, biological properties, and acid dissociation constant of novel naphthoquinone–triazole hybrids, Bioorg. Chem. 105 (2020), 104441, https://doi.org/10.1016/j.bioorg.2020.104441.

[38] T. Qin, Y.Y. Ma, C.E. Dong, W.L. Wu, Y.Y. Feng, S. Yang, J. Bin Su, X.X. Si, X. J. Wang, D.H. Shi, Design, synthesis, cytotoxicity evaluation and molecular docking studies of 1,4-naphthoquinone derivatives, J. Mol. Struct. 1263 (2022), 133067, https://doi.org/10.1016/J.MOLSTRUC.2022.133067.

[39] S.M. Ansari, G. Khanum, M.U.S. Bhat, M.A. Rizvi, N.U.D. Reshi, M.A. Ganie, S. Javed, B.A. Shah, Studies towards investigation of Naphthoquinone-based scaffold with crystal structure as lead for SARS-CoV-19 management, J. Mol. Struct. 1283 (2023), 135256, https://doi.org/10.1016/J.MOLSTRUC.2023.135256.

[40] A. Alimohammadi, H. Mostafavi, M. Mahdavi, Thiourea derivatives based on the dapsone-naphthoquinone hybrid as anticancer and antimicrobial agents: *in vitro* screening and molecular docking studies, ChemistrySelect 5 (2020) 847–852, https://doi.org/10.1002/SLCT.201903179.

[41] M. Gemili, Y. Nural, E. Keleş, B. Aydıner, N. Seferoğlu, M. Ülger, E. Şahin, S. Erat, Z. Seferoğlu, Novel highly functionalized 1,4-naphthoquinone 2-iminothiazole hybrids: synthesis, photophysical properties, crystal structure, DFT studies, and anti(myco)bacterial/antifungal activity, J. Mol. Struct. 1196 (2019) 536–546, https://doi.org/10.1016/j.molstruc.2019.06.087.

[42] R.M. Costa Souza, L.M.L. Montenegro Pimentel, L.K.M. Ferreira, V.R.A. Pereira, A. C.D.S. Santos, W.M. Dantas, C.J.O. Silva, R.M. De Medeiros Brito, J.L. Andrade, V. F. De Andrade-Neto, R.T. Fujiwara, L.L. Bueno, V.A. Silva Junior, L. Pena, C. A. Camara, B. Rathi, R.N. De Oliveira, Biological activity of 1,2,3-triazole-2-amino-1,4-naphthoquinone derivatives and their evaluation as therapeutic strategy for malaria control, Eur. J. Med. Chem. 255 (2023), 115400, https://doi.org/10.1016/j.ejmech.2023.115400.

[43] M.T. Riaz, M. Yaqub, Z. Shafiq, A. Ashraf, M. Khalid, P. Taslimi, R. Tas, B. Tuzun, İ. Gulçin, Synthesis, biological activity and docking calculations of bis-

naphthoquinone derivatives from Lawsone, Bioorg. Chem. 114 (2021), 105069, https://doi.org/10.1016/J.BIOORG.2021.105069.
[44] S. Hosseini, S.A. Pourmousavi, M. Mahdavi, P. Taslimi, Synthesis, and *in vitro* biological evaluations of novel naphthoquinone conjugated to aryl triazole acetamide derivatives as potential anti-Alzheimer agents, J. Mol. Struct. 1255 (2022), 132229, https://doi.org/10.1016/j.molstruc.2021.132229.
[45] Y. Yu, A. Liu, G. Dhawan, H. Mei, W. Zhang, K. Izawa, V.A. Soloshonok, J. Han, Fluorine-containing pharmaceuticals approved by the FDA in 2020: synthesis and biological activity, Chin. Chem. Lett. 32 (2021) 3342–3354, https://doi.org/10.1016/j.cclet.2021.05.042.
[46] B. Qi, F. Wang, H. He, M. Fan, L. Hu, L. Xiong, G. Gong, S. Shi, X. Song, Identification of (S)-1-(2-(2,4-difluorophenyl)-4-oxothiazolidin-3-yl)-3-(4-((7-(3-(4-ethylpiperazin-1-yl)propoxy)-6-methoxyquinolin-4-yl)oxy)-3,5-difluorophenyl) urea as a potential anti-colorectal cancer agent, Eur. J. Med. Chem. 239 (2022), 114561, https://doi.org/10.1016/j.ejmech.2022.114561.
[47] F. Bi, L. Guo, Y. Wang, H. Venter, S.J. Semple, F. Liu, S. Ma, Design, synthesis and biological activity evaluation of novel 2,6-difluorobenzamide derivatives through FtsZ inhibition, Bioorg. Med. Chem. Lett. 27 (2017) 958–962, https://doi.org/10.1016/j.bmcl.2016.12.081.
[48] Y.-S. Wang, T.-K. Yeh, W.-C. Chang, J.-P. Liou, Y.-M. Liu, W.-C. Huang, 2,6-Difluorobenzamide derivatives as store-operated calcium channel (SOC) inhibitors, Eur. J. Med. Chem. 243 (2022), 114773, https://doi.org/10.1016/j.ejmech.2022.114773.
[49] Y. Zhou, X. Xu, F. Wang, H. He, B. Qi, Discovery of 4-((4-(4-(3-(2-(2,6-difluorophenyl)-4-oxothiazolidin-3-yl)ureido)-2-fluorophenoxy)-6-methoxyquinolin-7-yl)oxy)-N,N-diethylpiperidine-1-carboxamide as kinase inhibitor for the treatment of colorectal cancer, Bioorg. Chem. 106 (2021), 104511, https://doi.org/10.1016/j.bioorg.2020.104511.
[50] Y. Demir, C. Türkeş, Ö.İ. Küfrevioğlu, Ş. Beydemir, Molecular docking studies and the effect of fluorophenylthiourea derivatives on glutathione-dependent enzymes, Chem. Biodivers. 20 (2023), e202200656, https://doi.org/10.1002/cbdv.202200656.
[51] Y. Nural, E. Karasu, E. Keleş, B. Aydıner, N. Seferoğlu, Ç. Efeoğlu, E. Şahin, Z. Seferoğlu, Synthesis of novel acylthioureas bearing naphthoquinone moiety as dual sensor for high-performance naked-eye colorimetric and fluorescence detection of CN− and F− ions and its application in water and food samples, Dye. Pigm. 198 (2022), 110006, https://doi.org/10.1016/j.dyepig.2021.110006.
[52] Bruker, APEX2, SAINT and SADABS, APEX II, Bruker AXS Inc, Madison, Wisconsin, USA, 2012.
[53] G.M. Sheldrick, SHEXS-2013, SHEXS-2013, University of Göttingen., 2013.
[54] J.A. Verpoorte, S. Mehta, J.T. Edsall, Esterase activities of human carbonic anhydrases B and C, J. Biol. Chem. 242 (1967) 4221–4229, https://doi.org/10.1016/S0021-9258(18)95800-X.
[55] C. Türkeş, M. Arslan, Y. Demir, L. Çoçaj, A. Rifati Nixha, Ş. Beydemir, Synthesis, biological evaluation and *in silico* studies of novel N-substituted phthalazine sulfonamide compounds as potent carbonic anhydrase and acetylcholinesterase inhibitors, Bioorg. Chem. 89 (2019), 103004, https://doi.org/10.1016/j.bioorg.2019.103004.
[56] B. Sever, C. Türkeş, M.D. Altıntop, Y. Demir, Ş. Beydemir, Thiazolyl-pyrazoline derivatives: *in vitro* and *in silico* evaluation as potential acetylcholinesterase and carbonic anhydrase inhibitors, Int. J. Biol. Macromol. 163 (2020) 1970–1988, https://doi.org/10.1016/j.ijbiomac.2020.09.043.
[57] G.L. Ellman, K.D. Courtney, V. Andres, R.M. Featherstone, A new and rapid colorimetric determination of acetylcholinesterase activity, Biochem. Pharmacol. 7 (1961) 88–95, https://doi.org/10.1016/0006-2952(61)90145-9.
[58] Z. Köksal, Z. Alım, S. Bayrak, İ. Gülçin, H. Özdemir, Investigation of the effects of some sulfonamides on acetylcholinesterase and carbonic anhydrase enzymes, J. Biochem. Mol. Toxicol. 33 (2019), https://doi.org/10.1002/jbt.22300.
[59] H.E. Aslan, Y. Demir, M.S. Özaslan, F. Türkan, Ş. Beydemir, Ö.I. Küfrevioğlu, The behavior of some chalcones on acetylcholinesterase and carbonic anhydrase activity, Drug Chem. Toxicol. 42 (2019) 634–640, https://doi.org/10.1080/01480545.2018.1463242.
[60] H. Lineweaver, D. Burk, The determination of enzyme dissociation constants, J. Am. Chem. Soc. 56 (1934) 658–666, https://doi.org/10.1021/ja01318a036.
[61] S. Chakravarty, K.K. Kannan, Drug-protein interactions: refined structures of three sulfonamide drug complexes of human carbonic anhydrase I enzyme, J. Mol. Biol. 243 (1994) 298–309, https://doi.org/10.1006/JMBI.1994.1655.
[62] C. Türkeş, Carbonic anhydrase inhibition by antiviral drugs *in vitro* and *in silico*, J. Mol. Recognit. 36 (2023) e3063, https://doi.org/10.1002/jmr.3063.
[63] K.H. Sippel, A.H. Robbins, J. Domsic, C. Genis, M. Agbandje-McKenna, R. McKenna, High-resolution structure of human carbonic anhydrase II complexed with acetazolamide reveals insights into inhibitor drug design, Acta Crystallogr. Sect. F Struct. Biol. Cryst. Commun. 65 (2009) 992–995, https://doi.org/10.1107/S1744309109036665.
[64] Ö. Güleç, C. Türkeş, M. Arslan, Y. Demir, B. Dincer, A. Ece, Ş. Beydemir, Novel beta-lactam substituted benzenesulfonamides: *in vitro* enzyme inhibition, cytotoxic activity and *in silico* interactions, J. Biomol. Struct. Dyn. (2023) 1–19, https://doi.org/10.1080/07391102.2023.2240889.
[65] K.V. Dileep, K. Ihara, C. Mishima-Tsumagari, M. Kukimoto-Niino, M. Yonemochi, K. Hanada, M. Shirouzu, K.Y.J. Zhang, Crystal structure of human acetylcholinesterase in complex with tacrine: implications for drug discovery, Int. J. Biol. Macromol. 210 (2022) 172–181, https://doi.org/10.1016/j.ijbiomac.2022.05.009.
[66] M. Erdoğan, M. Serdar Çavuş, H. Muğlu, H. Yakan, C. Türkeş, Y. Demir, Ş. Beydemir, Synthesis, theoretical, *in silico* and *in vitro* biological evaluation studies of new thiosemicarbazones as enzyme inhibitors, Chem. Biodivers. 20 (2023), e202301063, https://doi.org/10.1002/cbdv.202301063.
[67] F. Nachon, E. Carletti, C. Ronco, M. Trovaslet, Y. Nicolet, L. Jean, P.-Y. Renard, Crystal structures of human cholinesterases in complex with huprine W and tacrine: elements of specificity for anti-Alzheimer's drugs targeting acetyl- and butyryl-cholinesterase, Biochem. J. 453 (2013) 393–399, https://doi.org/10.1042/BJ20130013.
[68] C. Türkeş, S. Akocak, M. Işık, N. Lolak, P. Taslimi, M. Durgun, İ. Gülçin, Y. Budak, Ş. Beydemir, Novel inhibitors with sulfamethazine backbone: synthesis and biological study of multi-target cholinesterases and α-glucosidase inhibitors, J. Biomol. Struct. Dyn. 40 (2022) 8752–8764, https://doi.org/10.1080/07391102.2021.1916599.
[69] Schrödinger, Protein Preparation Wizard, In (Version 2023-2), Schrödinger, LLC, New york, NY, 2023. https://www.schrodinger.com/.
[70] D. Osmaniye, C. Türkeş, Y. Demir, Y. Özkay, Ş. Beydemir, Z.A. Kaplancıklı, Design, synthesis, and biological activity of novel dithiocarbamate-methylsulfonyl hybrids as carbonic anhydrase inhibitors, Arch. Pharm. (Weinheim) 355 (2022), https://doi.org/10.1002/ardp.202200132.
[71] Schrödinger, LigPrep, In (Version 2023-2), Schrödinger, LLC, New York, NY, 2023. https://www.schrodinger.com/.
[72] Y. Demir, C. Türkeş, M.S. Çavuş, M. Erdoğan, H. Muğlu, H. Yakan, Ş. Beydemir, Enzyme inhibition, molecular docking, and density functional theory studies of new thiosemicarbazones incorporating the 4-hydroxy-3,5-dimethoxy benzaldehyde motif, Arch. Pharm. (Weinheim) 356 (2023), e202200554, https://doi.org/10.1002/ardp.202200554.
[73] C. Lu, C. Wu, D. Ghoreishi, W. Chen, L. Wang, W. Damm, G.A. Ross, M.K. Dahlgren, E. Russell, C.D. Von Bargen, R. Abel, R.A. Friesner, E.D. Harder, OPLS4: improving force field accuracy on challenging regimes of chemical space, J. Chem. Theory Comput. 17 (2021) 4291–4300, https://doi.org/10.1021/acs.jctc.1c00302.
[74] C. Türkeş, Y. Demir, Ş. Beydemir, Infection medications: assessment *in-vitro* glutathione S-transferase inhibition and molecular docking study, ChemistrySelect 6 (2021) 11915–11924, https://doi.org/10.1002/slct.202103197.
[75] Schrödinger, Schrödinger Release 2023-3, Epik, 2023, 2023.
[76] J.C. Shelley, A. Cholleti, L.L. Frye, J.R. Greenwood, M.R. Timlin, M. Uchimaya, Epik: a software program for pK a prediction and protonation state generation for drug-like molecules, J. Comput. Aid. Mol. Des. 21 (2007) 681–691, https://doi.org/10.1007/s10822-007-9133-z.
[77] Schrödinger, Schrödinger Release 2023-3, SiteMap, 2023.
[78] T. Halgren, New method for fast and accurate binding-site identification and analysis, Chem. Biol. Drug Des. 69 (2007) 146–148, https://doi.org/10.1111/j.1747-0285.2007.00483.x.
[79] B. Çalışkan, Y. Demir, C. Türkeş, Ophthalmic drugs: *in vitro* paraoxonase 1 inhibition and molecular docking studies, Biotechnol. Appl. Biochem. 69 (2022) 2273–2283, https://doi.org/10.1002/bab.2284.
[80] Schrödinger, Schrödinger Release 2023-3, 2023. Receptor Grid Generation.
[81] C. Kakakhan, C. Türkeş, Ö. Güleç, Y. Demir, M. Arslan, G. Özkemahlı, Ş. Beydemir, Exploration of 1,2,3-triazole linked benzenesulfonamide derivatives as isoform selective inhibitors of human carbonic anhydrase, Bioorg. Med. Chem. 77 (2023), 117111, https://doi.org/10.1016/j.bmc.2022.117111.
[82] Schrödinger, Schrödinger Release 2023-3, Maestro, LLC, New York, NY, 2023.
[83] Y. Demir, F.S. Tokalı, E. Kalay, C. Türkeş, P. Tokalı, O.N. Aslan, K. Şendil, Ş. Beydemir, Synthesis and characterization of novel acyl hydrazones derived from vanillin as potential aldose reductase inhibitors, Mol. Divers. 27 (2023) 1713–1733, https://doi.org/10.1007/s11030-022-10526-1.
[84] Schrödinger, Schrödinger Release 2023-3, Glide, LLC, New York, NY, 2023.
[85] H. Yakan, H. Muğlu, C. Türkeş, Y. Demir, M. Erdoğan, M.S. Çavuş, Ş. Beydemir, A novel series of thiosemicarbazone hybrid scaffolds: design, synthesis, DFT studies, metabolic enzyme inhibition properties, and molecular docking calculations, J. Mol. Struct. 1280 (2023), 135077, https://doi.org/10.1016/j.molstruc.2023.135077.
[86] R.A. Friesner, J.L. Banks, R.B. Murphy, T.A. Halgren, J.J. Klicic, D.T. Mainz, M. P. Repasky, E.H. Knoll, M. Shelley, J.K. Perry, D.E. Shaw, P. Francis, P.S. Shenkin, Glide: a new approach for rapid, accurate docking and scoring. 1. Method and assessment of docking accuracy, J. Med. Chem. 47 (2004) 1739–1749, https://doi.org/10.1021/jm0306430.
[87] T.A. Halgren, R.B. Murphy, R.A. Friesner, H.S. Beard, L.L. Frye, W.T. Pollard, J. L. Banks, Glide: a new approach for rapid, accurate docking and scoring. 2. Enrichment factors in database screening, J. Med. Chem. 47 (2004) 1750–1759, https://doi.org/10.1021/jm030644s.
[88] Schrödinger, Schrödinger Release 2023-3, QikProp, LLC, New York, NY, 2023.
[89] A. Buza, C. Türkeş, M. Arslan, Y. Demir, B. Dincer, A.R. Nixha, Ş. Beydemir, Discovery of novel benzenesulfonamides incorporating 1,2,3-triazole scaffold as carbonic anhydrase I, II, IX, and XII inhibitors, Int. J. Biol. Macromol. 239 (2023), 124232, https://doi.org/10.1016/j.ijbiomac.2023.124232.
[90] Y. Nural, M. Gemili, N. Seferoglu, E. Sahin, M. Ulger, H. Sari, Synthesis, crystal structure, DFT studies, acid dissociation constant, and antimicrobial activity of methyl 2-(4-chlorophenyl)-7a-((4-chlorophenyl)carbamothioyl)-1-oxo-5,5-diphenyl-3-thioxo-hexahydro-1H-pyrrolo[1,2-*e*]imidazole-6-carboxylate, J. Mol. Struct. 1160 (2018) 375–382, https://doi.org/10.1016/j.molstruc.2018.01.099.
[91] C.A. Lipinski, F. Lombardo, B.W. Dominy, P.J. Feeney, Experimental and computational approaches to estimate solubility and permeability in drug discovery and development settings, Adv. Drug. Deliv. Rev. 64 (2012) 4–17, https://doi.org/10.1016/j.addr.2012.09.019.
[92] E.M. Duffy, W.L. Jorgensen, Prediction of Properties from Simulations: Free energies of solvation in hexadecane, octanol, and water, J. Am. Chem. Soc. 122 (2000) 2878–2888, https://doi.org/10.1021/ja993663t.

[93] K. Mazák, B. Noszál, Advances in microspeciation of drugs and biomolecules: species-specific concentrations, acid-base properties and related parameters, J. Pharm. Biomed. Anal. 130 (2016) 390–403, https://doi.org/10.1016/j.jpba.2016.03.053.

[94] Y. Altun, F. Köseoğlu, H. Demirelli, İ. Yılmaz, A. Çukurovalı, N. Kavak, Potentiometric studies on nickel (II), copper (II) and zinc (II) metal complexes with new schiff bases containing cyclobutane and thiazole groups in 60% dioxane-water mixture, J. Braz. Chem. Soc. 20 (2009) 299–308, https://doi.org/10.1590/S0103-50532009000200015.

[95] C. Öğretir, Ş. Demirayak, M. Duran, Spectroscopic determination and evaluation of acidity constants for some drug precursor 2-amino-4-(3- or 4-substituted phenyl) thiazole derivatives, J. Chem. Eng. Data 55 (2010) 1137–1142, https://doi.org/10.1021/je9005739.

[96] K.C. Gross, P.G. Seybold, Substituent effects on the physical properties and pKa of aniline, Int. J. Quantum Chem. 80 (2000) 1107–1115, https://doi.org/10.1002/1097-461X(2000)80:4/5<1107::AID-QUA60>3.0.CO;2-T.